



HAL
open science

Unraveling the Environment Influence in Bistable Spin-Crossover Particles Using Magnetometric and Calorimetric First-Order Reverse Curves

Radu Tanasa, Cristian Enachescu, Jérôme Laisney, Denis Morineau, Alexandru Stancu, Marie-Laure Boillot

► **To cite this version:**

Radu Tanasa, Cristian Enachescu, Jérôme Laisney, Denis Morineau, Alexandru Stancu, et al.. Unraveling the Environment Influence in Bistable Spin-Crossover Particles Using Magnetometric and Calorimetric First-Order Reverse Curves. *Journal of Physical Chemistry C*, 2019, 123 (15), pp.10120-10129. 10.1021/acs.jpcc.9b00768 . hal-02143863

HAL Id: hal-02143863

<https://univ-rennes.hal.science/hal-02143863>

Submitted on 29 May 2019

HAL is a multi-disciplinary open access archive for the deposit and dissemination of scientific research documents, whether they are published or not. The documents may come from teaching and research institutions in France or abroad, or from public or private research centers.

L'archive ouverte pluridisciplinaire **HAL**, est destinée au dépôt et à la diffusion de documents scientifiques de niveau recherche, publiés ou non, émanant des établissements d'enseignement et de recherche français ou étrangers, des laboratoires publics ou privés.

1
2
3
4
5
6
7
8
9
10
11
12
13
14
15
16
17
18
19
20
21
22
23
24
25
26
27
28
29
30
31
32
33
34
35
36
37
38
39
40
41
42
43
44
45
46
47
48
49
50
51
52
53
54
55
56
57
58
59
60

Unravelling The Environment Influence In Bistable Spin Crossover Particles Using Magnetometric And Calorimetric First Order Reverse Curves

Radu Tanasa¹, Cristian Enachescu^{1}, Jérôme Laisney^{2‡}, Denis Morineau^{3*}, Alexandru Stancu¹, Marie-Laure Boillot^{2*}*

¹ Faculty of Physics, "Alexandru Ioan Cuza" University, 700506, Iasi, Romania;

²Institut de Chimie Moléculaire et des Matériaux d'Orsay, Univ. Paris-Sud, Université Paris-Saclay, CNRS, 91405 Orsay, France;

³ Institut de Physique de Rennes, CNRS, Université de Rennes 1, UMR 6251, 35042 Rennes France;

[‡] Present address, Department of Plant and Soil Sciences, University of Kentucky, Lexington, Kentucky, 40546, USA.

1
2
3
4
5
6
7
8 *corresponding authors: cristian.enachescu@uaic.ro , marie-laure.boillot@u-psud.fr,
9
10
11 denis.morineau@univ-rennes1.fr
12
13
14
15
16
17
18
19

20 ABSTRACT

21
22
23
24
25 First-order reversal curves (FORC) method is used here to analyze the unexpected
26
27
28
29 change of memory characteristic of spin-crossover microparticles embedded in glass-
30
31
32 forming or semi-crystalline matrices, reflected in the larger hysteresis loop compared to
33
34
35
36 the bulk. The huge reversibility shown by the reversal curves was attributed to an effect
37
38
39 of matrix, implying a variable external pressure and a cut off – switch on mechanism of
40
41
42
43 particle–matrix interactions. The FORC analysis indicates that heating and cooling
44
45
46
47 processes in the case of matrix-embedded spin-crossover systems are driven by different
48
49
50
51 mechanisms. In complement of standard magnetometry measurements, a calorimetry
52
53
54
55 method, which demands an alternative method to extract FORC distributions, is
56
57
58
59
60

1
2
3 introduced for tracking the signature of the composite transformation, to understand and
4
5
6
7 to control the role of embedding matrices.
8
9

16 INTRODUCTION

20 First-order reversal curves (FORC) method became recently a powerful tool for the
21
22
23
24 characterization of hysteretic behavior in a broad range of materials, starting with
25
26
27
28 magnetic materials¹ and continuing with ferroelectric² or geological samples³. For more
29
30
31 than a decade, FORC method has been applied for understanding the properties of
32
33
34
35 spin-crossover compounds⁴⁻⁷ as well. Spin-crossover (SC) compounds⁸⁻⁹ are inorganic
36
37
38
39 molecular compounds, having a d^4 - d^7 transition metal as central ion and situated in an
40
41
42 octahedral ligand field. Due to classical thermodynamic reasons¹⁰, they can switch
43
44
45
46 between two states, a high spin (HS) state – stable at high temperature and a low spin
47
48
49 (LS) state, stable at lower temperature. The two states have different magnetic, optical,
50
51
52
53 mechanical and volume properties making them suitable for applications.¹¹⁻¹³ In the
54
55
56
57 case of strong elastic interactions between spin-crossover units, the transition is
58
59
60

1
2
3 accompanied by a thermal hysteresis loop. Though different as origin, the spin-
4
5
6
7 crossover thermal hysteresis presents some common features with the hysteresis of
8
9
10 magnetic materials, which allowed their study using methods initially developed for
11
12
13 ferromagnetism, such as the theoretical Preisach model¹⁴ which is the starting point of
14
15
16
17 the experimental FORC technique⁴⁻⁵. One of these common features is the existence of
18
19
20
21 spin-like domains, which has been proven for spin-crossover complexes in X-Ray
22
23
24 Diffraction¹⁵ and Raman spectroscopy¹⁶ or optical microscopy¹⁷⁻¹⁸ experiments.
25
26
27

28
29 Initial studies using the FORC method on spin-crossover complexes targeted the
30
31
32 thermal hysteresis and they successfully described the spin-like domain properties in
33
34
35
36 terms of physical parameters, such as the coercivity (intra- and inter-domain
37
38
39 interactions) or bias (energy gap)⁵. Further analysis implied specific cases of kinetic
40
41
42 light-induced thermal hysteresis⁶, systems with dopants¹⁹ or pressure hysteresis⁷, while
43
44
45
46 a method to disentangle between kinetic and static components has been proposed as
47
48
49
50 well.²⁰ The main advantage of the FORC method is that it can be applied directly to
51
52
53
54 experimental data like a characterization tool.
55
56
57
58
59
60

1
2
3 The behavior of spin-crossover nano- and microparticles showed several differences
4
5 compared to bulk compounds. Thus, spin-crossover nanoparticles thermal transition is
6
7 more gradual, shifted towards lower temperature and sometimes incomplete, while the
8
9 hysteresis loop has a smaller width, vanishes²¹ or even may reappear²²⁻²³ in case of a
10
11 few nanometer size objects. Thus, FORC method was more difficult to apply and the
12
13 number of studies remains still quite low. Still, the study of nanoparticles present some
14
15 interesting features, for instance an important reversible component in the hysteretic
16
17 behavior²⁴, that could be assigned to an anhysteretic effect associated to over-critical
18
19 size particles as in the case of polycrystalline samples.
20
21
22
23
24
25
26
27
28
29
30
31
32
33
34
35

36 Spin crossover nano- or microparticles were generally used as coated with stabilizers or
37
38 dispersed in various media (surfactants, polymers, glass-forming matrices). The
39
40 presence of such environment dramatically changes the overall properties of the
41
42 nanoparticles system.^{23, 25} This initial observation triggered a number of both
43
44 experimental²⁶ and theoretical studies²⁷⁻²⁹, to figure out the effect of matrix/particle
45
46 interactions. Moreover an unexpected widening of hysteresis loop have been detected
47
48
49
50
51
52
53
54
55
56
57
58
59
60

1
2
3 in the case of microparticles embedded in various matrices, which was described as an
4
5
6
7 effect of SC particles-matrix interactions.³⁰ Experimental reversal curves showed no
8
9
10 evidence for a cooperative process but a huge and surprising reversibility, explained as
11
12
13 a cut-off / switch on of interactions, determined by the spin dependent particle volume
14
15
16
17 and by the state of the surrounding matrix.³¹⁻³²
18
19
20
21

22 Therefore, there is a need for more advanced experimental techniques to probe
23
24
25 efficiently the changes in the switch behavior of the particles while interacting with the
26
27
28 matrix. The FORC technique appears to be the most appropriate, as it is a powerful
29
30
31
32 sensitive detector of intra- and inter-particles interactions changes.⁵
33
34
35
36

37 Here we use the FORC method to perform an in-depth study of hysteretic behavior of
38
39
40 spin crossover Fe(II) microparticles dispersed in matrices, focusing on the notable
41
42
43 deviations from the bulk materials. In addition to standard magnetometry technique
44
45
46 showing the unexpected strong effects of matrix/particle interactions, we introduce here
47
48
49
50 a complementary experimental technique based on calorimetric measurements. This
51
52
53
54 technique enables to probe the change of state of both particles and matrix separately
55
56
57
58
59
60

1
2
3 and therefore to better disentangle the behavior inherent to the embedding matrices and
4
5
6
7 that of the spin-crossover microparticles. The paper is organized as follows: first we
8
9
10 present magnetic and calorimetric studies of the thermal transition of spin-crossover
11
12
13 microparticles embedded in glass-forming (or semi-crystalline) matrices – nujol, eicosan
14
15
16 and glycerol–, then we present FORCs and FORC distributions in both magnetometric
17
18
19 and calorimetric measurements. Methods and results are then discussed.
20
21
22
23
24

25 EXPERIMENTAL SECTION

26 a) Magnetic study of the thermal transition vs. the matrix nature

27
28
29
30
31
32
33
34 Microparticles of $\text{Fe}(\text{phen})_2(\text{NCS})_2$ have been synthesized according to a procedure
35
36
37 described in Ref.³³ Different characterizations including TEM, IR, Magnetic and XRD
38
39
40 measurements confirmed the formation of pure crystalline $1.6(0.4) \times 1.6(0.4) \times 0.35(0.15)$
41
42
43 μm^3 particles of the spin-transition compound (see SI for TEM images and powder X-
44
45
46 Ray diagrams). The powder was then dispersed³⁰ in eicosan, nujol or glycerol with a
47
48
49 percentage of 2% (magnetism), 49 % (or 4 %, calorimetry) spin active compound with
50
51
52 respect to the dispersant. The solidification of eicosan leads to semi-crystalline domains
53
54
55
56
57
58
59
60

1
2
3 at $T_m = 310$ K as proved by X-ray diffraction. Nujol, a glass-forming oil ($T_g = 200$ K),
4
5
6
7 shows a partial recrystallization between 205 and 270 K³⁴, while the glass-transition
8
9
10 temperature of glycerol is $T_g \sim 185$ -192 K.³⁵ The magnetic data have been obtained
11
12
13 using a SQUID magnetometer (Quantum Design) at a constant magnetic field (5000
14
15
16 Oe), providing a susceptibility signal used to infer the high-spin fraction (denoted here
17
18
19 as n_{HS}), which is the ratio of molecules in the HS state over the total number of
20
21
22 molecules. The temperature sweeping rate was 0.3 K·min⁻¹; several sweeping rates
23
24
25
26
27 were considered and no dependence on this parameter was detected.
28
29
30

31
32 In Fig. 1, we present thermal transition curves for $\text{Fe}(\text{phen})_2(\text{NCS})_2$ as powder and as
33
34
35
36
37
38
39
40
41
42
43
44
45
46
47
48
49
50
51
52
53
54
55
56
57
58
59
60
61
62
63
64
65
66
67
68
69
70
71
72
73
74
75
76
77
78
79
80
81
82
83
84
85
86
87
88
89
90
91
92
93
94
95
96
97
98
99
100
101
102
103
104
105
106
107
108
109
110
111
112
113
114
115
116
117
118
119
120
121
122
123
124
125
126
127
128
129
130
131
132
133
134
135
136
137
138
139
140
141
142
143
144
145
146
147
148
149
150
151
152
153
154
155
156
157
158
159
160
161
162
163
164
165
166
167
168
169
170
171
172
173
174
175
176
177
178
179
180
181
182
183
184
185
186
187
188
189
190
191
192
193
194
195
196
197
198
199
200
201
202
203
204
205
206
207
208
209
210
211
212
213
214
215
216
217
218
219
220
221
222
223
224
225
226
227
228
229
230
231
232
233
234
235
236
237
238
239
240
241
242
243
244
245
246
247
248
249
250
251
252
253
254
255
256
257
258
259
260
261
262
263
264
265
266
267
268
269
270
271
272
273
274
275
276
277
278
279
280
281
282
283
284
285
286
287
288
289
290
291
292
293
294
295
296
297
298
299
300
301
302
303
304
305
306
307
308
309
310
311
312
313
314
315
316
317
318
319
320
321
322
323
324
325
326
327
328
329
330
331
332
333
334
335
336
337
338
339
340
341
342
343
344
345
346
347
348
349
350
351
352
353
354
355
356
357
358
359
360
361
362
363
364
365
366
367
368
369
370
371
372
373
374
375
376
377
378
379
380
381
382
383
384
385
386
387
388
389
390
391
392
393
394
395
396
397
398
399
400
401
402
403
404
405
406
407
408
409
410
411
412
413
414
415
416
417
418
419
420
421
422
423
424
425
426
427
428
429
430
431
432
433
434
435
436
437
438
439
440
441
442
443
444
445
446
447
448
449
450
451
452
453
454
455
456
457
458
459
460
461
462
463
464
465
466
467
468
469
470
471
472
473
474
475
476
477
478
479
480
481
482
483
484
485
486
487
488
489
490
491
492
493
494
495
496
497
498
499
500
501
502
503
504
505
506
507
508
509
510
511
512
513
514
515
516
517
518
519
520
521
522
523
524
525
526
527
528
529
530
531
532
533
534
535
536
537
538
539
540
541
542
543
544
545
546
547
548
549
550
551
552
553
554
555
556
557
558
559
560
561
562
563
564
565
566
567
568
569
570
571
572
573
574
575
576
577
578
579
580
581
582
583
584
585
586
587
588
589
590
591
592
593
594
595
596
597
598
599
600
601
602
603
604
605
606
607
608
609
610
611
612
613
614
615
616
617
618
619
620
621
622
623
624
625
626
627
628
629
630
631
632
633
634
635
636
637
638
639
640
641
642
643
644
645
646
647
648
649
650
651
652
653
654
655
656
657
658
659
660
661
662
663
664
665
666
667
668
669
670
671
672
673
674
675
676
677
678
679
680
681
682
683
684
685
686
687
688
689
690
691
692
693
694
695
696
697
698
699
700
701
702
703
704
705
706
707
708
709
710
711
712
713
714
715
716
717
718
719
720
721
722
723
724
725
726
727
728
729
730
731
732
733
734
735
736
737
738
739
740
741
742
743
744
745
746
747
748
749
750
751
752
753
754
755
756
757
758
759
760
761
762
763
764
765
766
767
768
769
770
771
772
773
774
775
776
777
778
779
780
781
782
783
784
785
786
787
788
789
790
791
792
793
794
795
796
797
798
799
800
801
802
803
804
805
806
807
808
809
810
811
812
813
814
815
816
817
818
819
820
821
822
823
824
825
826
827
828
829
830
831
832
833
834
835
836
837
838
839
840
841
842
843
844
845
846
847
848
849
850
851
852
853
854
855
856
857
858
859
860
861
862
863
864
865
866
867
868
869
870
871
872
873
874
875
876
877
878
879
880
881
882
883
884
885
886
887
888
889
890
891
892
893
894
895
896
897
898
899
900
901
902
903
904
905
906
907
908
909
910
911
912
913
914
915
916
917
918
919
920
921
922
923
924
925
926
927
928
929
930
931
932
933
934
935
936
937
938
939
940
941
942
943
944
945
946
947
948
949
950
951
952
953
954
955
956
957
958
959
960
961
962
963
964
965
966
967
968
969
970
971
972
973
974
975
976
977
978
979
980
981
982
983
984
985
986
987
988
989
990
991
992
993
994
995
996
997
998
999
1000

In Fig. 1, we present thermal transition curves for $\text{Fe}(\text{phen})_2(\text{NCS})_2$ as powder and as
microparticles dispersed in glycerol (main figure), and eicosan and nujol (inset).

While the polycrystalline powder of $\text{Fe}(\text{phen})_2(\text{NCS})_2$ (see SI for a TEM image) shows a
first-order spin-transition with a 2 K hysteresis loop centered around 176 K,
microcrystals of $\text{Fe}(\text{phen})_2(\text{NCS})_2$ dispersed in the selected matrices present a wider
hysteresis loop, with a progressive HS-to-LS transition curve shifted toward smaller
temperatures values and a LS-to-HS transition curve closely following the one obtained

1
2
3 with polycrystalline powder in absence of any dispersing medium. In addition, in the
4
5
6
7 case of particles dispersed in glycerol, two different hysteresis loops can be obtained
8
9
10 depending on the previous thermal treatment of the ensemble, respectively if the
11
12
13
14 composite was heated up to 190 or 250 K after the first cooling down. In order to
15
16
17 determine the exact nature of the phase formed by the glycerol matrix and to better
18
19
20 understand the effect of the thermal treatment on the shape of the hysteresis loop, we
21
22
23
24 have performed Differential Scanning Calorimetry (DSC) experiments, which shall be
25
26
27
28 presented in the next section.
29
30
31
32
33
34
35
36
37
38
39
40
41
42
43
44
45
46
47
48
49
50
51
52
53
54
55
56
57
58
59
60

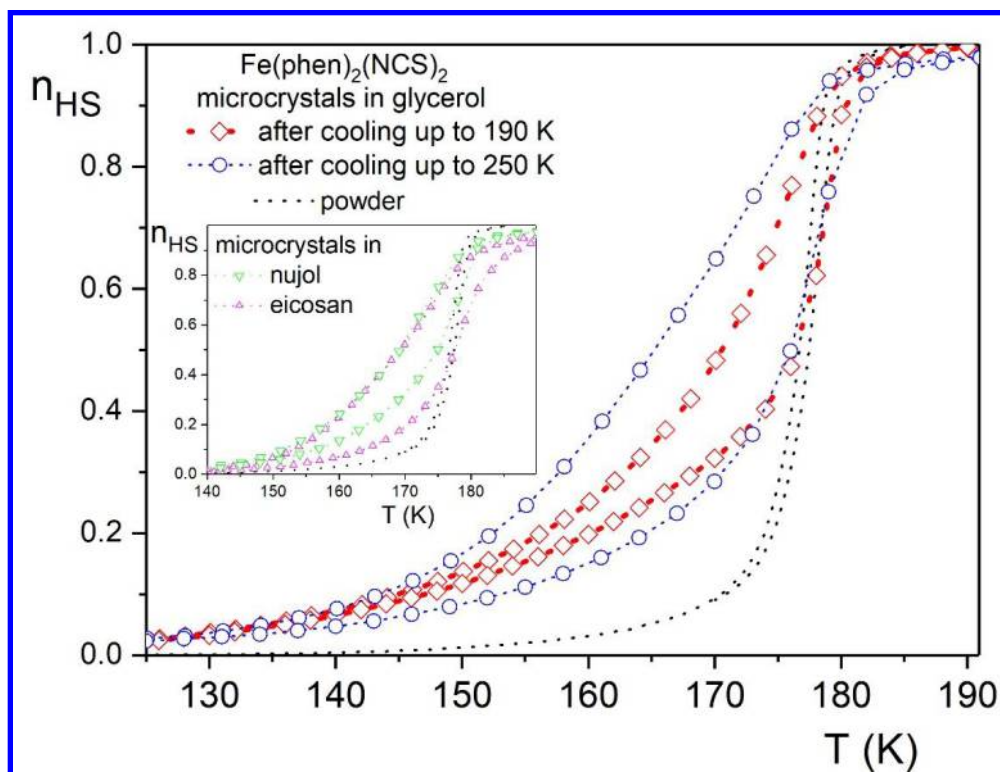


Figure 1 Major hysteresis loop (MHL) for $\text{Fe}(\text{phen})_2(\text{NCS})_2$ as polycrystalline powder (dotted line) and as dispersions of crystalline microparticles in glycerol after a first cooling down and heating up to 190 or 250 K (main figure) and as dispersions of crystalline microparticles in nujol and eicosan after a first cooling down and heating up to 190K (inset). All measurements have been performed with a temperature sweeping rate of $0.3 \text{ K}\cdot\text{min}^{-1}$.

b) Calorimetric study of the thermal transition

1
2
3 Besides magnetic measurements, calorimetric measurements were intensively used to
4
5
6
7 quantitatively evaluate the spin-crossover features³⁶⁻³⁹. Even the idea of spin-like
8
9
10 domains mentioned above was initially formulated in the pioneering years of spin-
11
12
13 crossover phenomenon studies by Sorai and Seki while looking at the heat anomaly
14
15
16 during first-order spin transition.⁴⁰ This kind of measurement was used to determine
17
18
19 relevant thermodynamical parameters, such as the enthalpy or the entropy changes
20
21
22 accompanying the thermal transition. We briefly acknowledge that DSC measures the
23
24
25 heat flow associated to the speed of progress of the spin transition, rather than the
26
27
28 instantaneous fraction of transformed spins measured by magnetometric methods. It is
29
30
31 sensitive to the phase transformations of both the microparticules (spin transition) and
32
33
34 the embedding matrix (crystallization, melting, glass transition). This is obviously not the
35
36
37 case for magnetometry and reflectometry measurements of spin-crossover compounds.
38
39
40
41
42
43
44
45 ⁷ Therefore, DSC method is especially suited to study composite systems. Applying
46
47
48 various thermal cycling techniques and more elaborate thermal treatments, one can
49
50
51 prepare the matrix in well-defined state (liquid, solid, glass) and assess its impact on the
52
53
54 microparticles spin-transition.
55
56
57
58
59
60

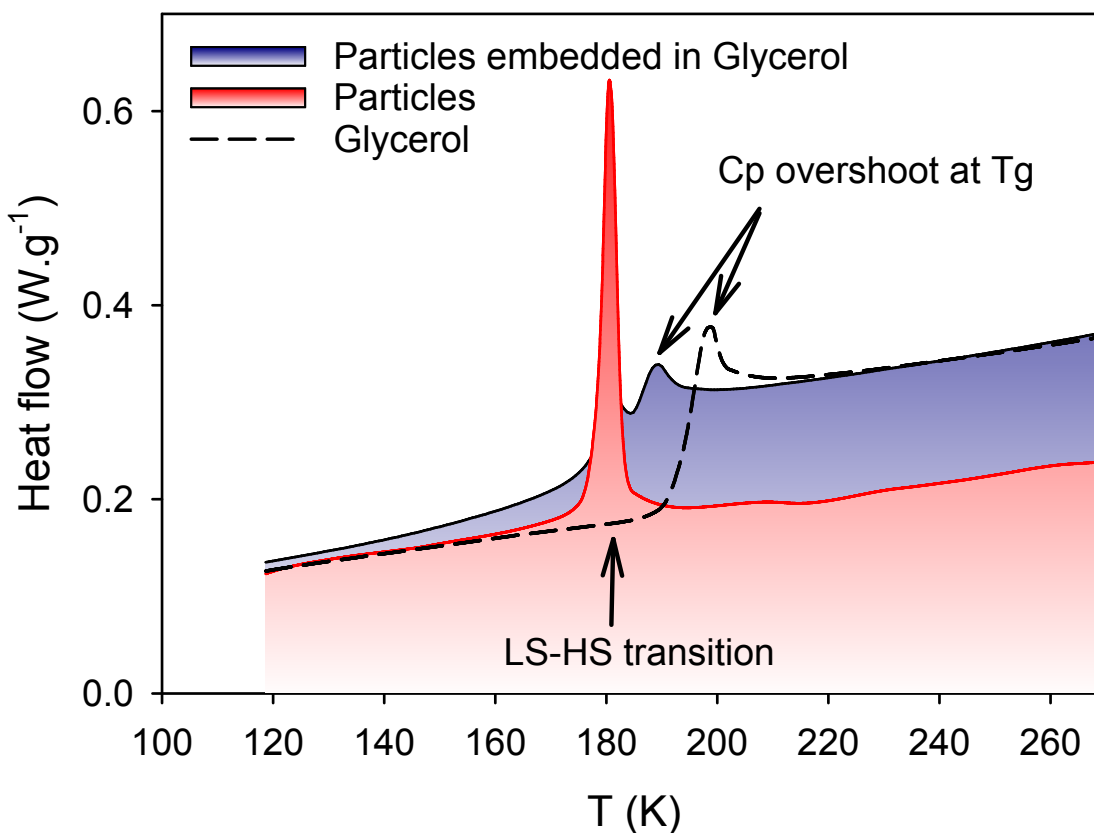
1
2
3
4 The calorimetric measurements were performed on a TA Instrument Q20 DSC
5
6
7 equipped with a liquid-nitrogen cooling system. Three different samples were prepared
8
9
10 and loaded in sealed aluminum pans: pure glycerol ($m = 6.37$ mg), free
11
12
13 Fe(phen)₂(NCS)₂ microparticles ($m = 3.3$ mg) -both considered as reference systems-
14
15
16 and a composite material formed by mixing Fe(phen)₂(NCS)₂ microparticles ($m = 20.8$
17
18 mg) with glycerol ($m = 21.5$ mg). The high mass ratio that was chosen for calibration
19
20
21 reasons also allowed us to check the preservation of the experimental observations
22
23
24 corresponding to 4 wt. %. By convention, the thermograms are presented with the
25
26
27 endothermic heat flow up. The heat flow was normalized with respect to the mass of
28
29
30 Fe(phen)₂(NCS)₂ for both the free microparticles and the microparticles embedded in
31
32
33 glycerol (so here equivalent to the mass of glycerol), while for pure glycerol, it was
34
35
36 normalized to the mass of glycerol. Two different scanning rates were applied (10
37
38
39 K·min⁻¹ and 0.5 K·min⁻¹) as specified in the text.
40
41
42
43
44
45
46
47
48
49

50 In Fig. 2, we present the thermograms of these three systems acquired during heating
51
52
53 at a constant rate (10 K·min⁻¹) from 110 to 270 K after an initial cooling down from 273
54
55
56
57
58
59
60

1
2
3 to 110 K at the same rate (not shown). For ensuring a better signal over noise
4
5
6
7 response, we used here a percentage of 49% of powder of microparticles with respect
8
9
10 to glycerol after checking the qualitative reproducibility of the phenomenon under
11
12
13 investigation (49 - 4% percentage). The thermogram of glycerol exhibits a jump of the
14
15
16 heat capacity ($\Delta C_p = 0.85 \text{ J}\cdot\text{g}^{-1}\cdot\text{K}^{-1}$) at the glass temperature $T_g = 194 \text{ K}$ ($T_{\text{onset}} = 192.3$
17
18
19 K), immediately followed by a small overshoot (see arrow), which is associated to
20
21
22 enthalpic relaxation effects around T_g . Glycerol is a prototypical glass-forming system,
23
24
25 and the crystallization could be easily avoided under these thermal conditions, as
26
27
28 shown in Fig. 3. The thermal behavior and the measured values are in agreement with
29
30
31 the literature for pure glycerol.⁴¹
32
33
34
35
36
37
38

39 The thermogram of free $\text{Fe}(\text{phen})_2(\text{NCS})_2$ microparticles exhibits a prominent
40
41
42 endothermic peak (see arrow) ($T_{\text{max}} = 180.5 \text{ K}$, $\Delta H = 11 \text{ J}\cdot\text{g}^{-1} = 5.9 \text{ kJ}\cdot\text{mol}^{-1}$) that
43
44
45 corresponds to the LS-HS transition. During cooling, a very similar exothermic peak was
46
47
48 observed at a nearby position, giving $T_{1/2} = 178.5 \text{ K}$ for the temperature of the center of
49
50
51
52
53 the hysteresis loop. This is in agreement with the first-order and highly cooperative
54
55
56
57
58
59
60

1
2
3 character of spin-transition discussed in the previous part concerning the magnetic
4
5
6
7 property. The measured ΔH and $T_{1/2}$ parameters are fully consistent with those reported
8
9
10 in the literature in case of the structurally characterized $\text{Fe}(\text{phen})_2(\text{NCS})_2$ materials in
11
12
13
14 the so-called form II. ⁴²
15
16
17
18
19
20
21
22
23
24
25



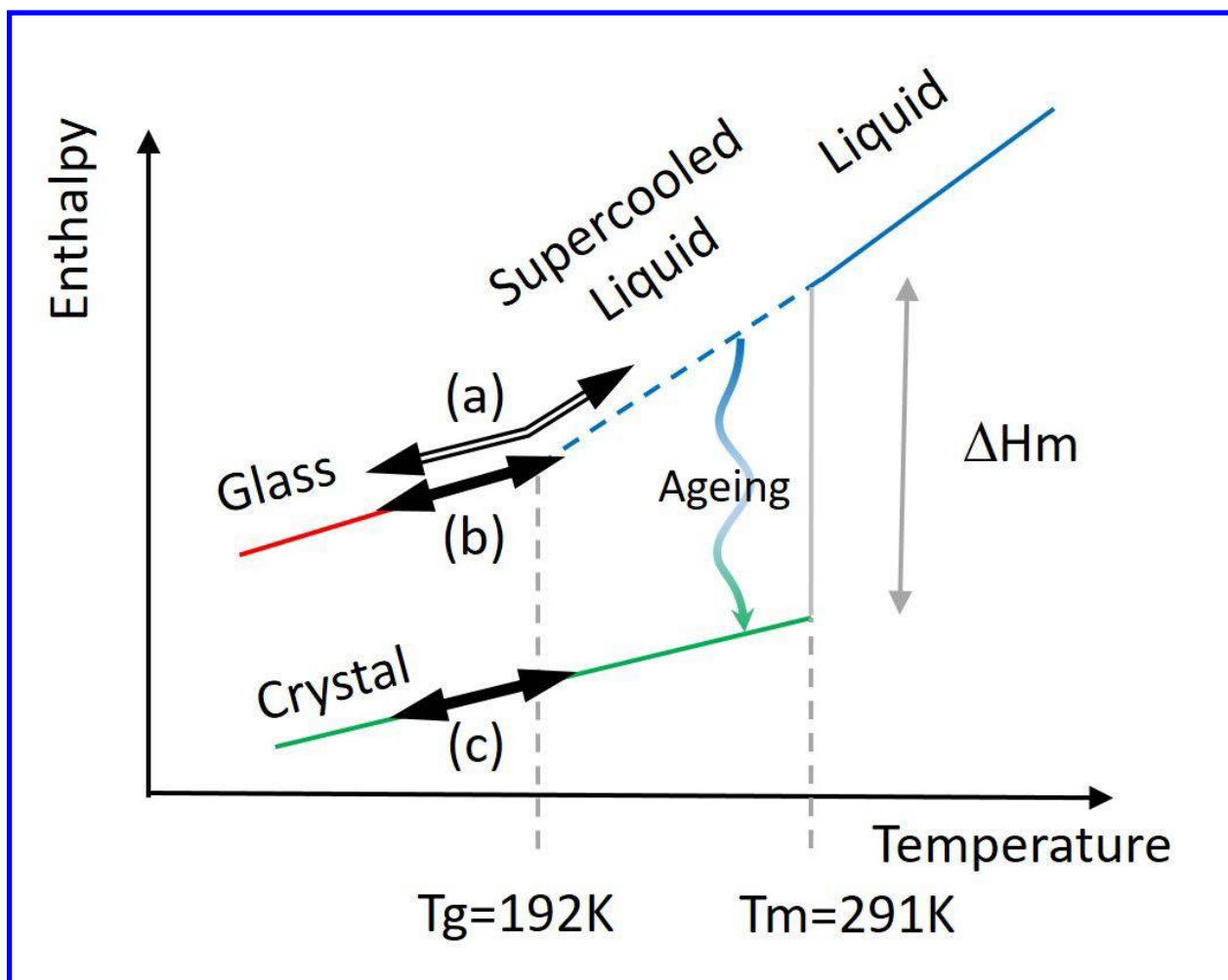
1
2
3 **Figure 2** DSC thermograms recorded on heating after a first cooling down from 273 to
4
5
6
7 110 K, with a temperature scanning rate of $10 \text{ K}\cdot\text{min}^{-1}$ for pure glycerol (dashed line),
8
9
10 free $\text{Fe}(\text{phen})_2(\text{NCS})_2$ microparticles (red shaded) and $\text{Fe}(\text{phen})_2(\text{NCS})_2$ microparticles
11
12
13
14 embedded in glycerol (blue line).
15
16
17

18 Next we discuss the thermogram of the $\text{Fe}(\text{phen})_2(\text{NCS})_2$ microparticles embedded in
19
20
21 glycerol (blue shaded curve in Fig. 2). It presents a jump of the heat capacity that is
22
23
24
25 actually a signature of the glass-to-liquid transition of the glycerol matrix. The glass
26
27
28 transition temperature is slightly shifted towards lower temperature with respect to the
29
30
31 pure glycerol, as indicated by the bump around 190 K instead of 198 K, which
32
33
34
35 corresponds to the overshoot of heat flux when crossing the glass-to-liquid transition. It
36
37
38
39 indicates that the particles may have a small plasticizing⁴³ influence on the dynamics of
40
41
42 supercooled glycerol – *the matrix itself has not only a complex behavior with an intrinsic*
43
44
45 *hysteresis of mechanical origin, but also it is influenced by the size and density of spin-*
46
47
48 *crossover microparticles.* More interestingly, this overshoot is preceded by a distinct
49
50
51
52
53 endothermic peak ($T_{\text{max}} = 181 \text{ K}$), indicating the LS-HS transition of the dispersed
54
55
56
57
58
59
60

1
2
3 microparticles. Despite a comparable position of the maximum peak, the transition of
4
5
6
7 the $\text{Fe}(\text{phen})_2(\text{NCS})_2$ microparticles embedded in glycerol occurs much more gradually
8
9
10 than for the free particles, feature which corresponds to magnetometry data. A
11
12
13
14 broadening of the peak is observed and its low temperature side spreads out down to
15
16
17 about 130 K. It illustrates the progressive character of the spin transition of embedded
18
19
20 particles – in other words the embedding destroys the cooperativity. So from these
21
22
23
24 DSC measurements, we can be infer that the matrix and the SC particles are strongly
25
26
27
28 coupled.
29
30

31
32 In the following, we shall explain the differences in thermal transition observed for
33
34
35
36 glycerol environment after heating up to 190 or 250 K. The different states of glycerol
37
38
39 are sketched in Fig. 3, where the enthalpy is plotted over the temperature. While
40
41
42 glycerol is solely liquid above the melting point ($T_m = 291$ K), it can exist in different
43
44
45
46 forms at lower temperature. Below T_m , the equilibrium phase is crystalline, but glycerol
47
48
49
50 can be usually supercooled in its metastable liquid state. On further cooling, the
51
52
53
54
55
56
57
58
59
60

1
2
3 viscosity of the supercooled liquid is too high to fulfill equilibrium, so that it is eventually
4
5
6
7 stuck into an out-of-equilibrium amorphous solid (glass transition $T_g = 192$ K).
8
9
10
11
12
13
14
15



16
17
18
19
20
21
22
23
24
25
26
27
28
29
30
31
32
33
34
35
36
37
38
39
40
41
42
43
44
45
46
47
48
49
50
51
52
53
54
55
56
57
58
59
60
Figure 3 Schematic representation of glycerol stable and metastable phases. The thermal treatments are shown by arrows: (a) cycling in the glassy and liquid phases in

1
2
3 the range 100-250 K, (b) cycling in glassy phase 100-190 K, and (c) cycling in the
4
5
6
7 crystal 100-190 K. (adapted from ⁴⁴)
8
9

10
11 In Fig. 4, we present the hysteresis loops recorded by DSC for two different cycling
12
13
14 conditions. The sample was firstly cooled down from 250 to 100 K (dashed line, noted
15
16
17 (a) in Fig. 3) and later cycled between 100 and 190 K (solid lines, noted (b) in Fig. 3). A
18
19
20 temperature rate of $0.5 \text{ K}\cdot\text{min}^{-1}$ was applied to facilitate comparison with the magnetic
21
22
23 measurements percentage. The first cooling branch shows sharp lines (spikes) that
24
25
26 dampen and disappear in the subsequent thermograms as long as the system is cycled
27
28
29 in the range 100-190 K, but they appear again during the first cooling if the system is
30
31
32 heated above 250K. If one excepts these spikes, weak exothermic signals are visible
33
34
35 when comparing the two thermal cycles. A first signal can be detected around 170 K
36
37
38
39 whatever the cycle, while a second one (magnified in S.I.) only appears in the range
40
41
42
43 140-150 K after a sample first cooling from 273 K. This small difference is systematic
44
45
46
47 and really significant as confirmed when zooming in and comparing different cycles (see
48
49
50
51
52
53
54
55
56
57
58
59
60 S.I.). In contrast, the heating branches cycled in the range 100-250 K and 100-190 K

are always superimposed. They do not show any apparent dependence on the thermal history of the system.

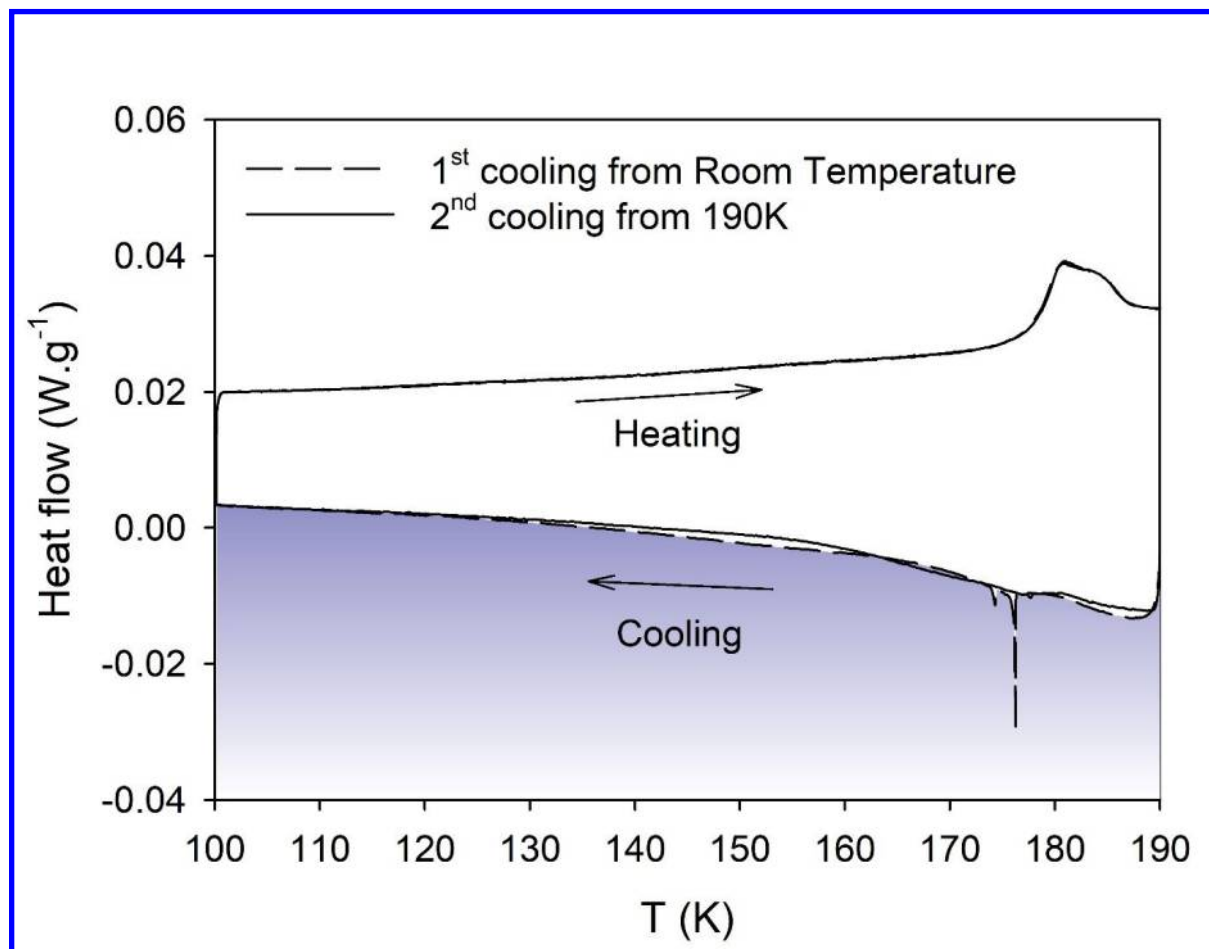


Figure 4 DSC thermograms of $\text{Fe}(\text{phen})_2(\text{NCS})_2$ microparticles embedded in glycerol recorded with a temperature scanning rate of $0.5 \text{ K} \cdot \text{min}^{-1}$ and with different cycling conditions. The two lower curves correspond to the cooling branches: a first cooldown after having heated the system above 250 K (dashed line) and a subsequent cooldown

1
2
3 after heating up to 190 K (solid line). The two upper curves correspond to the heating
4
5
6
7 branches (superimposed solid lines).
8
9

10
11 This behavior is in line with the magnetic measurements shown in Fig. 1, which also
12
13
14 indicated a clear variation of the cooling branch depending on the value of the upper
15
16
17
18 temperature. The origin of this behavior can be hypothesized from a recent DSC study
19
20
21
22 on glass-forming molecular systems.⁴⁵ Similar thermal spikes due to a discontinuity of
23
24
25 the thermal contact arising from the motion of seals aluminium pans were observed
26
27
28
29 during cooling of glassy materials. They were attributed to the formation of cracks in the
30
31
32 glassy phase well below T_g . Cracks arise from the sudden mechanical release of
33
34
35 stresses that develop during deep quenches. As such, they usually appear 50 K or
36
37
38
39 more below the glass-transition temperature. In S.I. we exemplify the broad peak by
40
41
42 focusing only on the cooling branch.
43
44
45

46
47 In the present study, the spikes appear only a few degrees below the glass transition of
48
49
50
51 glycerol. Under these mild conditions of supercooling, the glycerol matrix unexpectedly
52
53
54 developed a significant amount of residual mechanical stresses. We rather infer that
55
56
57
58
59
60

1
2
3 during the first cooling, the large volume contraction of the particles associated to the
4
5
6
7 spin transition could not be sustained by the embedding frozen amorphous solid. The
8
9
10 spikes associated to some degree of cracking of the matrix, and thus new free volumes,
11
12
13 is indicative of an irreversible change in the microparticles-matrix interactions which
14
15
16
17 necessarily impacts the spin crossover process as previously proposed (cutting-off of
18
19
20 elastic interactions). It also introduces extra environment distribution and possible
21
22
23 residual stress. The influence of non-relaxed particle-matrix interactions could explain
24
25
26
27 the higher depression of the HS-LS transition along the major hysteresis loop (MHL)
28
29
30 cooling branch (see exothermic broad peak in the range 140-150 K for the very first
31
32
33 curve starting from a thermally quenched glassy state). The initial state of the composite
34
35
36
37 (giving rise to elastic interactions and mechanical stresses) is recovered when the
38
39
40
41 matrix is allowed to relax in the non-viscous liquid phase at a temperature well above T_g
42
43
44 (approximately 250 K). These observations support the concepts of cut off/switch on of
45
46
47
48 particles-matrix interactions when cycling through the glass transition of matrices, which
49
50
51
52 were introduced recently in a mean-field model.³¹
53
54
55
56
57
58
59
60

c) FORC ANALYSIS OF THE THERMAL HYSTERESIS

In order to in-depth analyze the particle-matrix interactions, we have measured first-order reversal curves for microparticles embedded in glycerol, and for comparison purpose in eicosan and nujol. The FORCs are a specific class of minor hysteresis loops, for which the sweep of the input parameter, temperature here, is reversed once from one of the branches of the major hysteresis loop.

For a hysteretic cooperative spin transition, the warming/cooling types of FORC experiments should be distinguished, according to the sign of the thermal variations.

The measurements start at a sufficiently high/low temperature, such that the high/low temperature (HS/LS) domain structure is saturated. Then, temperature is lowered/raised until a given temperature T_R / T_R^* , the reversal temperature, and afterwards raised/lowered till reaching full HS/LS structures, in the heating/cooling mode respectively, as illustrated in Fig. 5 for the spin-crossover compound $[\text{Fe}_{0.6}\text{Zn}_{0.4}(\text{btr})_2(\text{NCS})_2] \cdot \text{H}_2\text{O}$. Typically, the experiment is repeated for several values of T_R / T_R^* , and $n_{\text{HS}}(T_r, T) / n_{\text{HS}}^*(T_r^*, T)$ values forms the FORC data (T being the

1
2
3 temperature at which the n_{HS} is measured for T_R , (T_R^*) reversal temperature in the
4
5
6
7 cooling (heating) branch). The possibility to generate various states within the major
8
9
10 hysteresis loop has been previously explained by the existence of the spin-like domains,
11
12
13 which behaves similar to a rectangular hysteresis loop, denoted as hysteron in the
14
15
16
17 Preisach formalism⁴⁶ (see inset of Fig. 5). The collection of the hysterons forms the so-
18
19
20 called Preisach distribution that, in magnetism, offers the statistical distribution either of
21
22
23 the switching fields or of the coercivities and the interactions fields of hysterons.^{5, 14}
24
25
26
27
28 Indeed, the width of the thermal hysteron represents the coercivity, related to intra-
29
30
31 domain cooperative interactions, while its shift relative to the average transition
32
33
34
35 temperature depends on inter-domain interactions.

36
37
38
39 The FORC distribution is defined as the second mixed derivative of these curves:
40
41
42

$$43 \quad \rho(T_R, T) = -\frac{\partial^2 n_{HS}(T_R, T)}{\partial T_R \partial T} \text{ and}$$

$$44 \quad \rho(T_R^*, T^*) = +\frac{\partial^2 n_{HS}(T_R^*, T^*)}{\partial T_R^* \partial T^*}$$

1
2
3 for heating and cooling modes, respectively.
4
5
6
7

8 The distribution of the switching temperatures is statistically stable in the case of non-
9
10
11 interacting domains, which makes the FORC distributions to be similar, to the so-called
12
13
14 Preisach distributions⁴⁷. Consequently, the FORC distributions in the cooling and
15
16
17 heating modes are expected to be the same, as is the case for the pure powder of the
18
19
20 spin crossover compound $[\text{Fe}(\text{btr})_2(\text{NCS})_2] \cdot \text{H}_2\text{O}$, whose typical FORC distributions are
21
22
23 indicated in Fig. 6. For an easier comparison, we have represented the heating
24
25
26 distribution in the classical Preisach half plane (below $T_R=T$ axis) and we have
27
28
29 translated the cooling distribution in the half-plane situated above the $T_R=T$ axis. We
30
31
32 notice then that the warming and cooling mode distributions tend to exhibit the expected
33
34
35 mirror symmetry with respect to the $T_R=T$ axis. This symmetry can be related to the
36
37
38 existence of only intra-domain interactions (a domain can be understood here as an
39
40
41
42
43
44
45
46 entire particle).
47
48
49
50
51
52
53
54
55
56
57
58
59
60

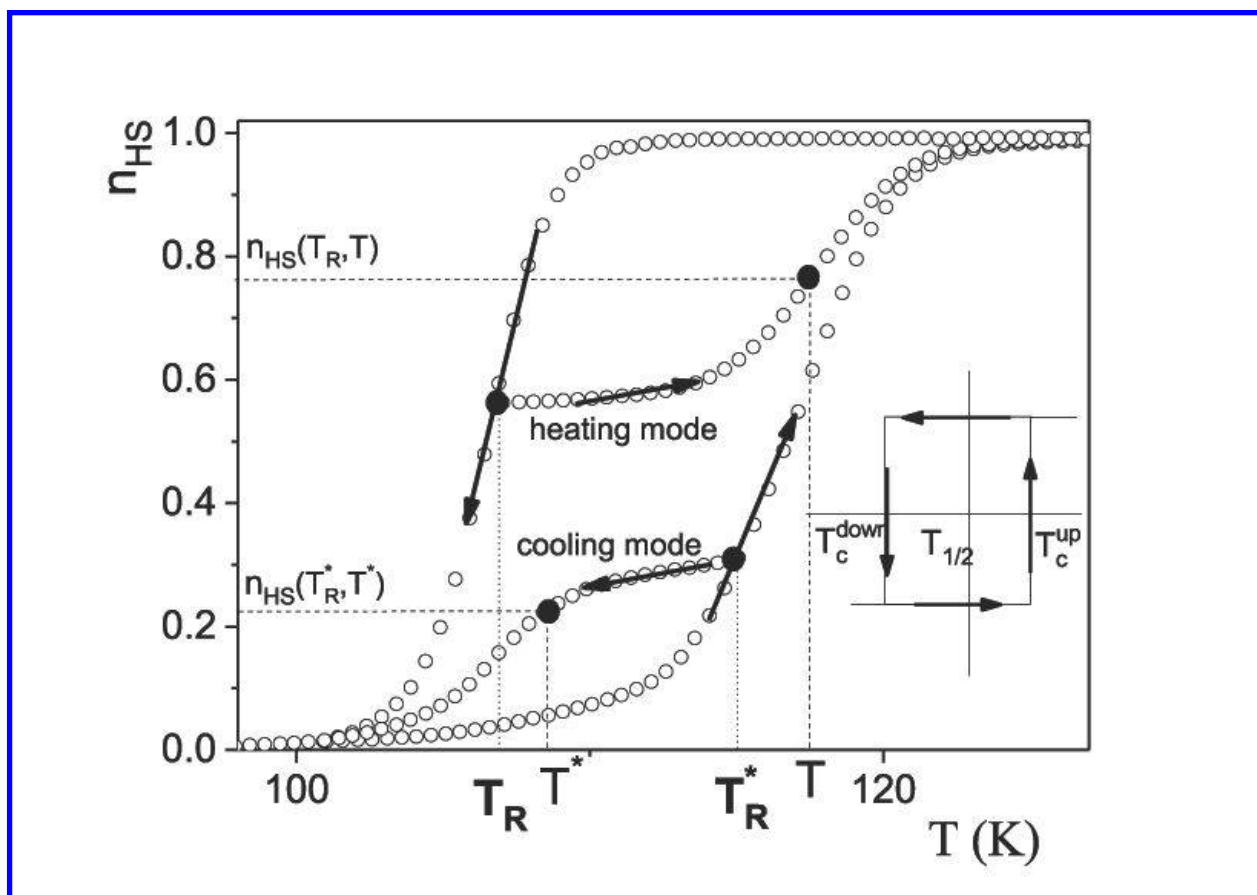


Figure 5 Examples of FORCs in warming and cooling modes; inset: typical hysteron

for cooperative interactions

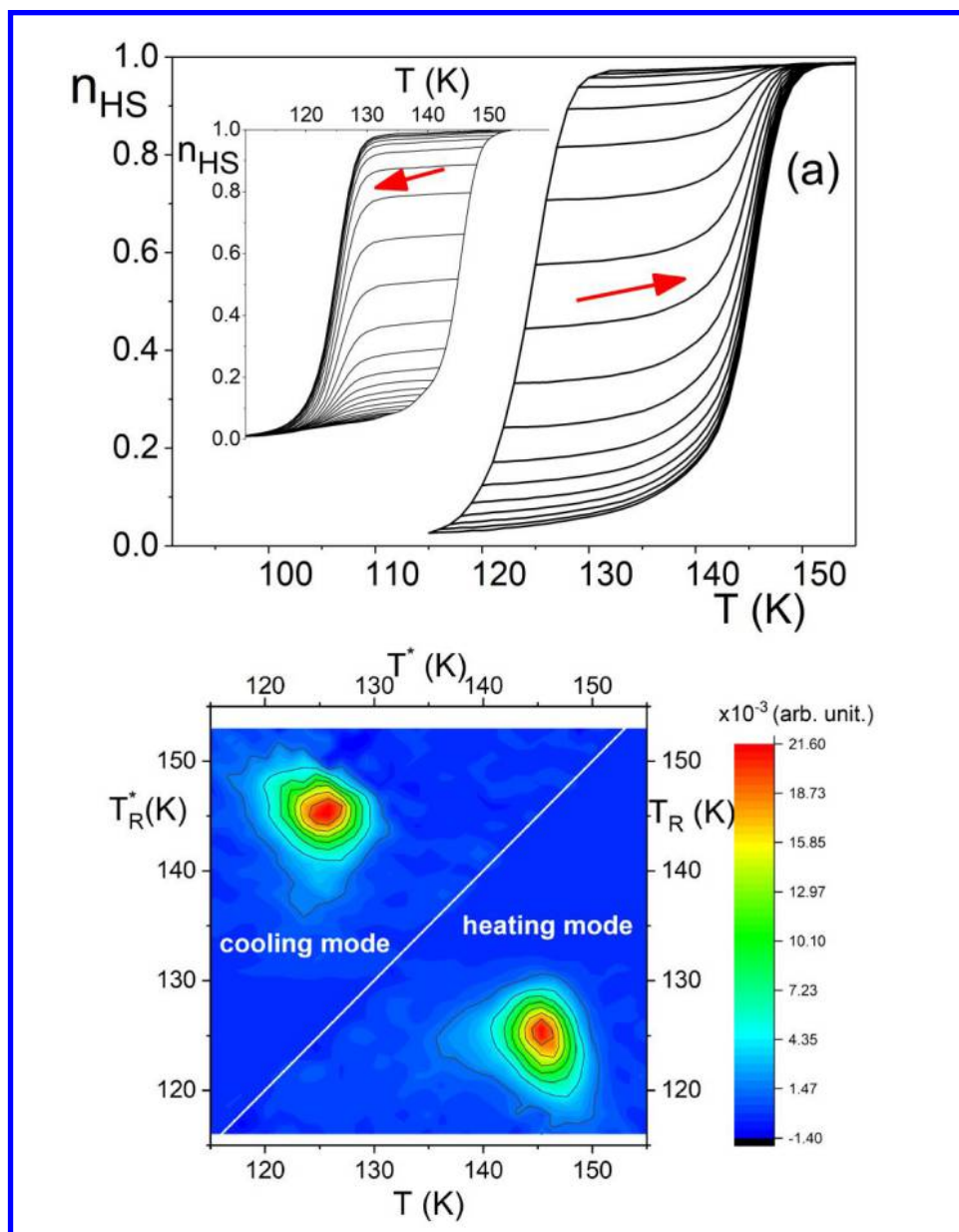


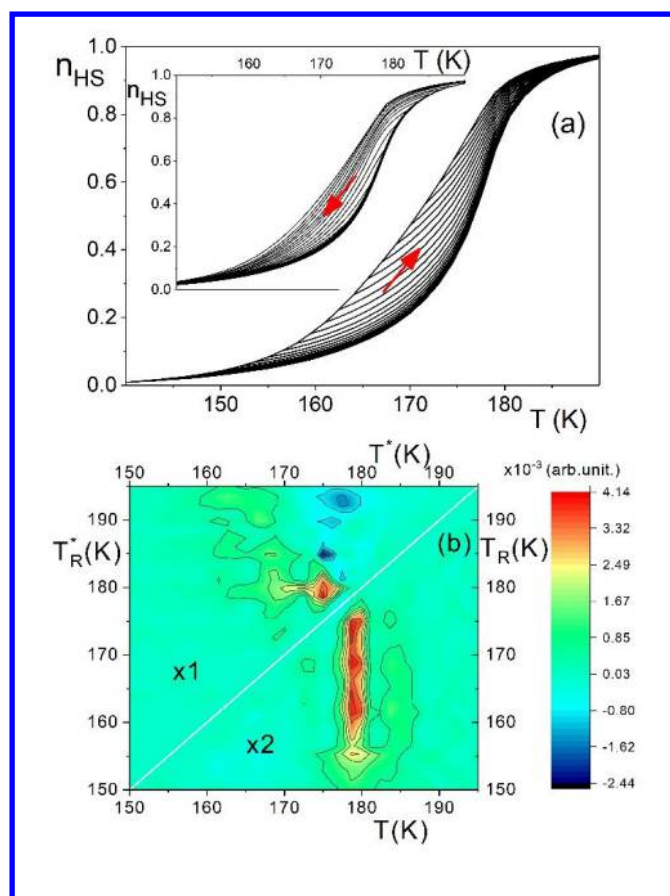
Figure 6 Typical FORCs in the case of powder spin-crossover compound

$[\text{Fe}(\text{btr})_2(\text{NCS})_2] \cdot \text{H}_2\text{O}$ ⁵ (a) Main figure: heating mode, inset: cooling mode. (b) FORC distributions for heating (lower side) and cooling modes (upper side).

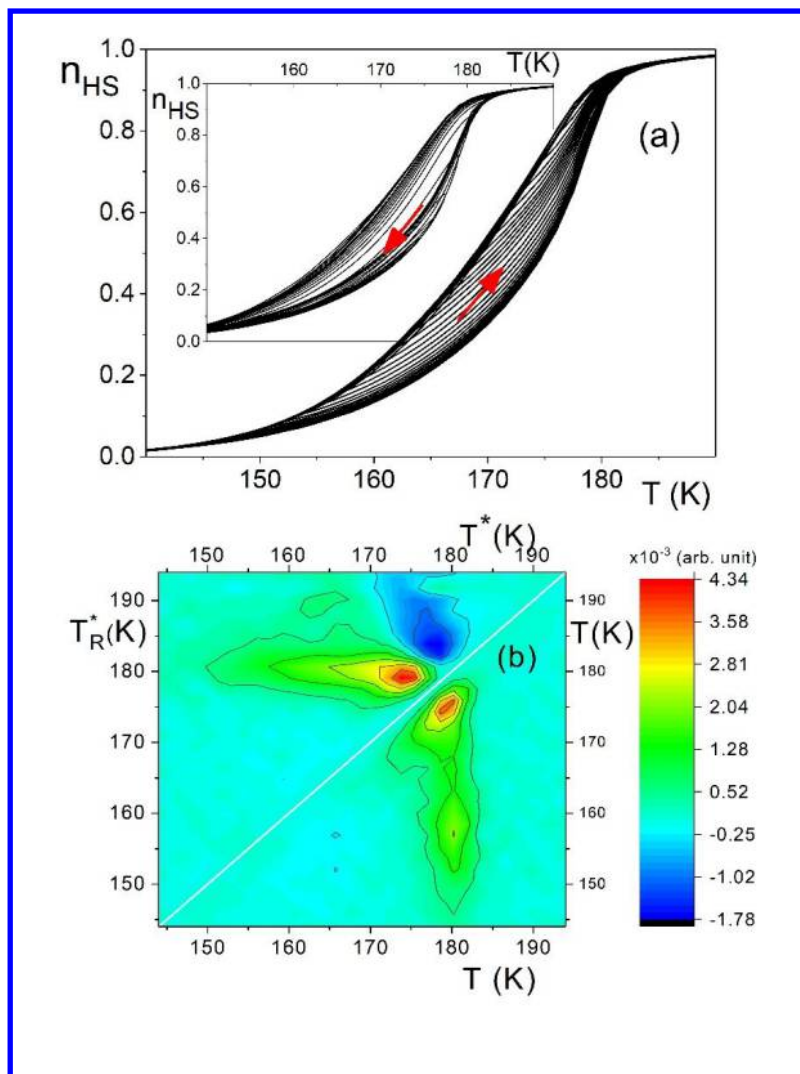
1
2
3
4 In Figs. 7-10, we present experimental FORCs - in panels a) for FORCs in the heating
5
6
7 mode and in the cooling mode (inset, corresponding to the ascending branch of the
8
9
10 MHL)- and in panels b), calculated FORC distributions, as the second order mixed
11
12
13 derivatives of n_{HS} for both modes for Fe(phen)₂(NCS)₂ embedded in eicosan, nujol and
14
15
16 glycerol respectively. In the case of glycerol, we distinguish in Figs. 9 and 10 the
17
18
19 heating mode FORCs obtained with the saturation heating temperature of 190 or 250 K
20
21
22 while for eicosan and nujol the saturation heating temperature in Fig. 7-8 is fixed at 190
23
24
25
26
27
28 K. In all situations, the FORCs exhibit the same peculiarities: they present a non-zero
29
30
31 slope in the vicinity of the reversal temperature, which is a sign of an important
32
33
34 reversible part. The latter that was not expected in case of pure sample⁵ could
35
36
37 unfortunately not be probed, because of the small hysteresis width of Fe(phen)₂(NCS)₂
38
39
40
41
42 in the bulk form.

43
44
45
46 In addition, we notice that the slope of reversal curves depends on the individual
47
48
49 reversal temperature. In the cooling mode, the FORCs are superimposable with the
50
51
52
53 major hysteresis loop up to an unusually high value of n_{HS} , approaching 0.4. For higher
54
55
56
57
58
59
60

1
2
3
4 n_{HS} values, they direct inside the hysteresis loop, but still remain far from a zero degree
5
6
7 slope. In a similar manner, the curves in the heating mode are very close to the major
8
9
10 hysteresis branch for a high value of n_{HS} , but start to enter into the hysteresis for
11
12
13
14 smaller n_{HS} .
15
16
17



1
2
3 **Figure 7** FORCs for $\text{Fe}(\text{phen})_2(\text{NCS})_2$ microparticles embedded in eicosan. (a) Main
4
5
6
7 figure: heating mode ($T_{\text{up}} = 190$ K), inset: cooling mode, $T_{\text{down}} = 140$ K). (b) FORC
8
9
10 distributions for heating (lower side, multiplied by 2) and cooling modes (upper side).



1
2
3 **Figure 8** FORCs for Fe(phen)₂(NCS)₂ microparticles embedded in nujol. (a) Main
4
5
6
7 figure: heating mode ($T_{\text{up}}=190$ K), inset: cooling mode ($T_{\text{down}} = 140$ K). (b) FORC
8
9
10 distributions for heating (lower side) and cooling modes (upper side).
11
12
13
14
15
16
17
18

19
20 The analysis of the FORC distributions (Fig. 7b-8b-9b-10b) reveals other interesting
21
22
23 features. As previously, we represent here the distribution in the two half planes of the
24
25
26 Preisach plane, separated by the $T_R = T$ line, with the heating distribution below and the
27
28
29 cooling distribution above this axis. The long shape of the main peaks is consistent with
30
31
32
33 the progressive widening of the hysteresis loop and could be also connected with
34
35
36 possible avalanche-type switchings.^{18, 25}
37
38
39
40

41
42 Regarding the different FORC distributions obtained for glycerol when cycling up to 190
43
44
45 and 250 K (Figs. 9, 10 b), they indicate that *the saturation should not be considered*
46
47
48 *only as the situation of a fully HS/LS structure, but also in connection with the*
49
50
51 *environment characteristics (liquid or solid nature, phase stabilization).* The differences
52
53
54
55 observed in case of nujol and eicosan, two paraffinic species, are also instructive. Nujol
56
57
58
59
60

1
2
3 becomes glassy while eicosan remains in a stable crystalline state. Accordingly, the
4
5
6
7 changes in their FORC distributions can be assigned to the differences in the
8
9
10 microparticles-matrix interactions as pointed above and thus to the elastic stability
11
12
13 characteristics of the two solidified matrices.⁴⁸
14
15
16
17

18 Another striking observation is the lack of the mirror symmetry in Figs. 7-10, in
19
20
21 opposition to the model bulk case where FORC distributions obtained in the heating and
22
23
24 cooling modes are rather similar (as shown in Fig. 6). This confirms first the effect of
25
26
27 variable interactions between the microparticles and the matrix (as here they replace
28
29
30 the classical interdomain interactions). Moreover it also shows that the processes at the
31
32
33 two major hysteresis loop branches are different, which confirms the assumption
34
35
36
37 previously made, when discussing only the major hysteresis cycle regarding a cut on
38
39
40 /switch off mechanism, which implies the existence of elastic forces between the spin
41
42
43 crossover microparticles and the surrounding matrix. Actually, in this case the physical
44
45
46 representation of spin-like domains is different from the single-crystal picture, as every
47
48
49 spin-crossover microparticle should be regarded as an independent single-domain
50
51
52
53
54
55
56
57
58
59
60

1
2
3
4 particle. As stated in the introduction, the volume of individual spin-crossover molecules
5
6
7 and consequently the whole microparticle volume diminish during the HS-to-LS
8
9
10 transition. Then, the microparticle-matrix interactions vary when the HS-to-LS transition
11
12
13 proceeds, due to the change of the spin-crossover microparticles volume, if the matrix is
14
15
16 not elastic enough to follow this change. The variation of the matrix-microparticle
17
18
19 interactions depends not only on the matrix elasticity and plasticity features, but also on
20
21
22 the microparticles size: larger the size, the larger is the absolute variation during the
23
24
25 transition and the variation of the distance between microparticle and matrix (see Fig.
26
27
28 11). This determines a variable distribution of interactions during HS-LS transition.
29
30
31
32
33
34 Finally, if the microparticle volume after the HS-LS transition is too small, the distance
35
36
37 between its surface and the matrix is so large that these interactions are suppressed
38
39
40 and the microparticle does not feel anymore the influence of matrix. However, we
41
42
43 expect that some small microparticles, whose absolute size variation is considerably
44
45
46 reduced, still keep, at least partially, their connections to the matrix (see Fig. 11 for a
47
48
49 schematic representation). We should notice that *the inter-domain interaction*
50
51
52
53
54
55
56 *distribution, as previously defined for spin-crossover compounds is replaced here with*
57
58
59
60

1
2
3
4 *particle-matrix interaction*. Therefore, while the HS-LS transition corresponds to a
5
6
7 particle interacting with the surrounding matrix, the LS-HS transition is closer to that of
8
9
10 an open boundary particle.
11

12
13
14
15 In the discussion above, we did not considered the presence of interactions between
16
17
18 particles mediated by the matrix^{23,49}, as in this case their possible effects are dampened
19
20
21 by the particle-matrix interactions. As shown above, the hysteresis obtained for
22
23
24
25 microparticles embedded in matrices is non-cooperative and therefore of a different
26
27
28 nature than the cooperative hysteresis of the bulk. Consequently, it is not determined by
29
30
31 the interactions mediated by the matrix (which should act similar to a bulk compound
32
33
34 where the spin-active molecules interact each other by elastic strains. Here we find out
35
36
37
38 new features elsewhere assigned to the formation of cracks of a glassy matrix (DSC
39
40
41 signals)⁴⁵ under the effect of internal shearing forces (solidification of pressure-
42
43
44 transmitting oils)⁵⁰ that are fully relevant with respect to this mechanism because of the
45
46
47
48
49 change of volume of SC particles.
50
51
52
53
54
55
56
57
58
59
60

1
2
3
4 Another interesting point is the presence of a negative region on the FORC
5
6
7 distributions in the cooling mode FORCs , which can be noticed for all matrices.
8
9

10 Generally speaking, negative regions in FORCs distributions were attributed to the
11
12
13
14 change in susceptibility variation between successive curves. Here the susceptibility is
15
16
17 given by the number of microparticles multiplied by their size. According to discussions
18
19
20 in previous paragraph, the larger microparticles are the first for which the interactions
21
22
23
24 with the matrix are cut during HS-LS transitions. Consequently, in this case a change in
25
26
27
28 susceptibility variation is possible, as a smaller number of large spin crossover
29
30
31 microparticles can count more than a larger number of average size spin crossover
32
33
34 microparticles. We have to strengthen that the origin of this negative distribution is
35
36
37
38 different from the negative distributions observed for rate dependent light induced
39
40
41
42 thermal hysteresis in spin crossover compounds⁶ or in the case of potential-driven
43
44
45 hysteresis in model electrochemical systems⁵¹ where it is due to the evolution of the system
46
47
48
49 toward the stable state, even after the direction of change of the control parameter has
50
51
52 changed.
53
54
55
56
57
58
59
60

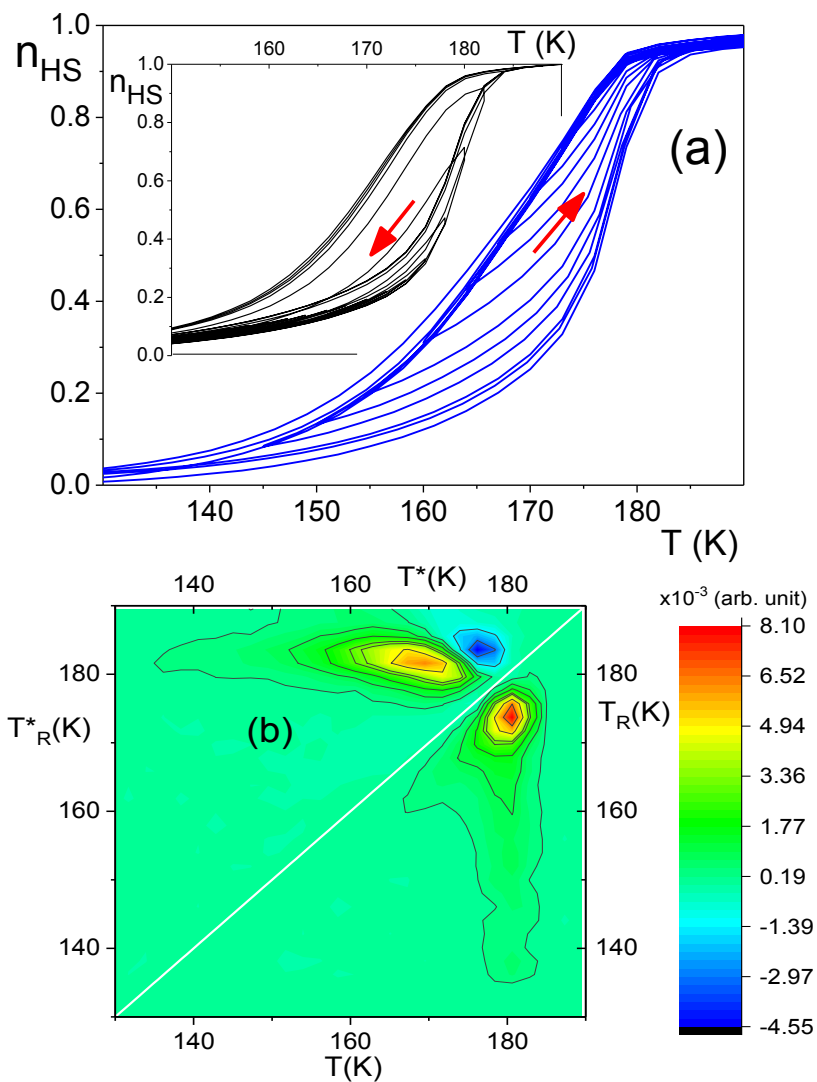


Figure 9 (a) FORCs for $\text{Fe}(\text{phen})_2(\text{NCS})_2$ microparticles embedded in glycerol for warming mode when cycling up to 250 K, (main figure) and cooling modes (inset) (b) Corresponding FORC distributions. The temperature scan rate was $0.3 \text{ K}\cdot\text{min}^{-1}$.

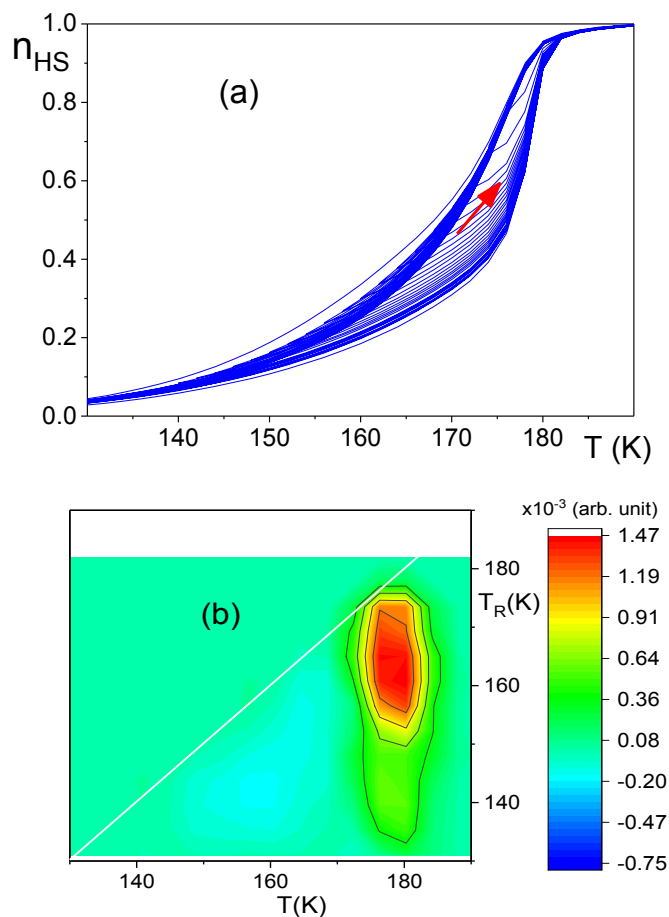


Figure 10 (a) FORCs for $\text{Fe}(\text{phen})_2(\text{NCS})_2$ microparticles embedded in glycerol for warming mode when cycling up to 190 K (main figure) (b) Corresponding FORC distributions. The temperature scan rate was $0.3 \text{ K}\cdot\text{min}^{-1}$.

We have to notice how the huge reversible component in the heating / cooling branch of the major hysteresis loop varies with the matrix preparation. The behavior in the case of $\text{Fe}(\text{phen})_2(\text{NCS})_2$ microparticles embedded in glycerol (Figs. 9, 10) is in part

1
2
3 similar with that of microparticles embedded in other matrices, but show some
4
5
6
7 peculiarities. The FORCs starting from the MHL cooling branch measured for
8
9
10 microparticles embedded in glycerol change when the temperature is cycled up to 250
11
12
13
14 K or up to 190 K. In the first case, the large reversible part in the cooling branch is
15
16
17 similar to the case of nujol, while in the second case, the reversible part is noticeably
18
19
20 smaller and the hysteresis loop slightly varies while cycling the temperature. According
21
22
23 to the calorimetric study (section II.B), it can be observed that the thermal cycling of the
24
25
26 composite up to 190 K results an irreversible loss of connectivity between particles and
27
28
29 matrix (matrix cracking). It can be suggested that both the decrease of the hysteresis
30
31
32 width shown in Fig. 4 and Fig. 9a. and the weaker FORC reversible component result
33
34
35 from the cracking (release of stresses) of the composites. This hypothesis is also
36
37
38 justified by the opposite trends observed when the temperature is cycled up to 250 K,
39
40
41
42 i.e. well above the glass-transition of the glycerol⁵² in conditions allowing the restoration
43
44
45
46
47
48 of the particles-matrix interactions.
49
50
51
52
53
54
55
56
57
58
59
60

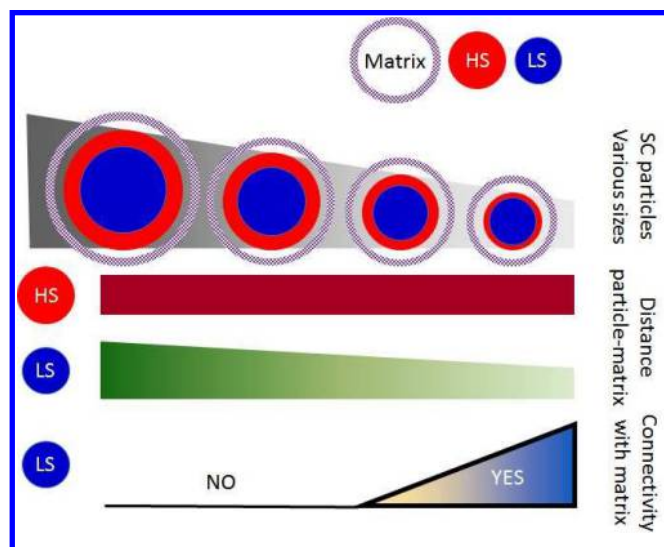


Figure 11 Schematic representation of particle-matrix interactions during HS-LS transition

d) FORC APPROACH/ANALYSIS: THE CALORIMETRIC INPUT

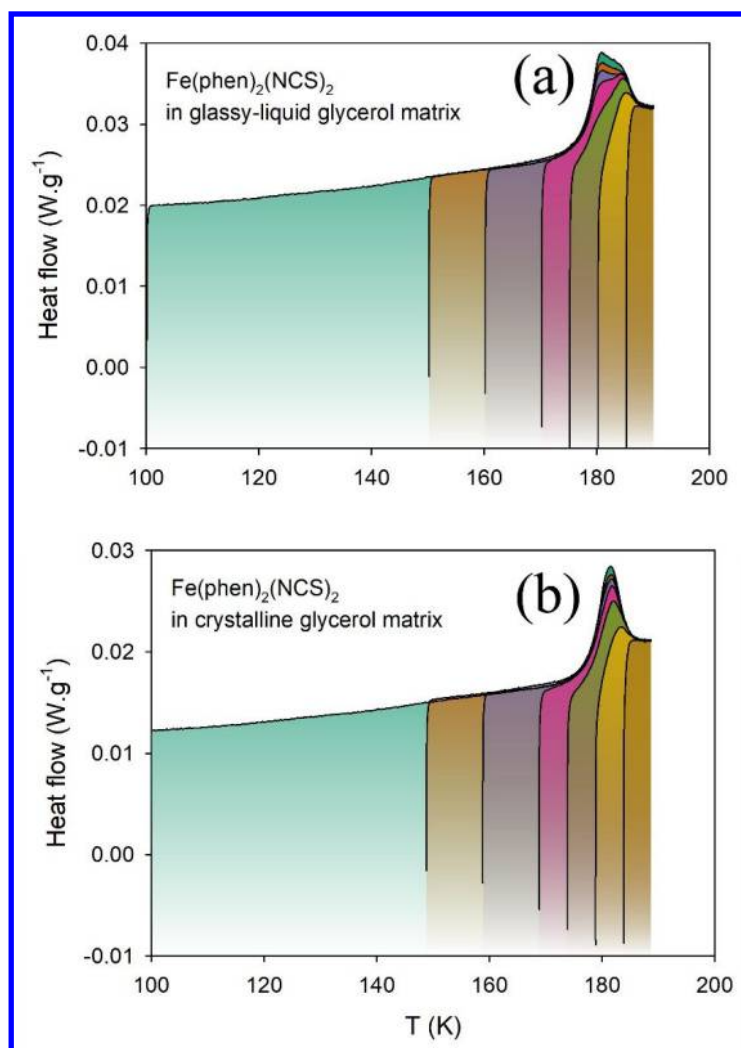
To confirm these findings, we have performed the same measurements based on the calorimetric technique, which provides a unique complement to the magnetometric FORCs method.

Considering the relevance of calorimetric measurements in the study of composite systems, we measured DSC-like FORCs. Mimicking the magnetometric experiments protocols discussed previously, we acquired thermograms in the heating mode, starting

1
2
3 from different lower temperatures (T_R in the range 100-190 K) to the same upper
4
5
6
7 temperature ($T_{up} = 190$ K). Both heating and cooling rates were set to $0.5 \text{ K}\cdot\text{min}^{-1}$.
8
9

10
11 In order to control the nature of the embedding matrix, two different thermal treatments
12
13
14 were applied prior to the DSC-like FORCs experiments. In the first case, the sample
15
16
17 was cooled down from 300 to 190 K and then cycled once between 100 and 190 K, in
18
19
20
21 order to prepare glycerol as a glassy matrix with relaxed elastic interactions (no residual
22
23
24 spikes as shown in Fig. 4) with the $\text{Fe}(\text{phen})_2(\text{NCS})_2$ microparticles. The subsequent
25
26
27
28 FORCs were measured for a glassy or very viscous liquid matrix (denoted as case (b) in
29
30
31
32 Fig. 3). In a second case, the sample was cooled down to 100 K and heated up to 270
33
34
35
36 K. This thermal treatment, which combines a deep quench in the glass and a
37
38
39 thermalization in the slightly supercooled liquid promotes the nucleation and the growth
40
41
42 of the crystalline phase. The subsequent FORCs were measured for a crystalline matrix
43
44
45
46 (denoted as case (c) in Fig. 3). It can be noted here that the behavior observed upon
47
48
49
50 the first cooling of the composite formed with the glassy or the crystalline matrix is
51
52
53
54 qualitatively unchanged.
55
56
57
58
59
60

1
2
3
4 The corresponding experimental FORCs measured while heating and that starts from
5
6
7 the cooling branch are shown in Fig. 12. The heat flow in Fig. 12a cumulates the
8
9
10 enthalpy LS-HS transition and the heat capacity jump of glass-liquid transition of
11
12
13
14 glycerol, while in Fig. 12b it accounts only for the enthalpy of LS-HS transition, glycerol
15
16
17 being crystallized.



1
2
3 **Figure 12** First Order Reversal Curves DSC thermograms in the heating mode for
4
5
6
7 composites of Fe(phen)₂(NCS)₂ microparticles embedded in glassy (a) and crystalline
8
9
10 (b) glycerol. Scanning rate: 0.5 K·min⁻¹.
11
12

13
14
15 The recording of calorimetric FORCs as heat capacity profiles opened the possibility to
16
17
18 represent FORC distributions for calorimetric data. However, there is an important
19
20
21 difference compared to the standard method for obtaining FORC distribution: as the
22
23
24 heat capacity already corresponds to the first derivative of the n_{HS} with the temperature,
25
26
27
28 only a single derivative is necessary in order to obtain the FORC distributions. The
29
30
31 concept of using of a single derivative to get the FORC diagram was theoretically
32
33
34 mentioned, however without practical implementation, more than a decade ago, in a
35
36
37 study concerning the voltammetric current in electrochemical FORC method⁵¹. One has
38
39
40
41
42
43 to strengthen that the specificity of this experiment is the quite large temperature step
44
45
46
47 between two consecutive reversal temperatures, due to the necessity to measure all
48
49
50 curves in the same conditions and to the time limitations of the experimental device; in
51
52
53 the same time the temperature step for a given value of the reversal temperature
54
55
56
57
58
59
60

1
2
3 should be small to obtain smooth curves (representing the first derivative of n_{HS} , as we
4
5
6
7 have explained before). In Fig. 12, we present FORC distributions in the heating mode
8
9
10 obtained using calorimetric data for $\text{Fe}(\text{phen})_2(\text{NCS})_2$ spin crossover microparticles
11
12
13 embedded in glassy (when cooling down from 190 K) and crystalline (when cooling
14
15
16 down from 270 K) glycerol compounds. Even not so preeminent, the maxima of the
17
18
19 distributions are situated at the same value as obtained from the magnetometry curves.
20
21
22
23
24 The high/sharp peaks along $T_R=T$ line (which are here more clear than in
25
26
27 magnetometric FORC discussed previously) are due to the reversible part of the curves.
28
29
30
31 In the case of the crystalline matrix, a kink is visible for the distribution around 180 K,
32
33
34 sign of a different interaction between the spin-crossover particle and the matrix. A
35
36
37
38 complete study of the peculiarities of the FORC technique obtained using the
39
40
41
42 calorimetry experiment will be realized in a further study.
43
44
45
46
47
48
49
50
51
52
53
54
55
56
57
58
59
60

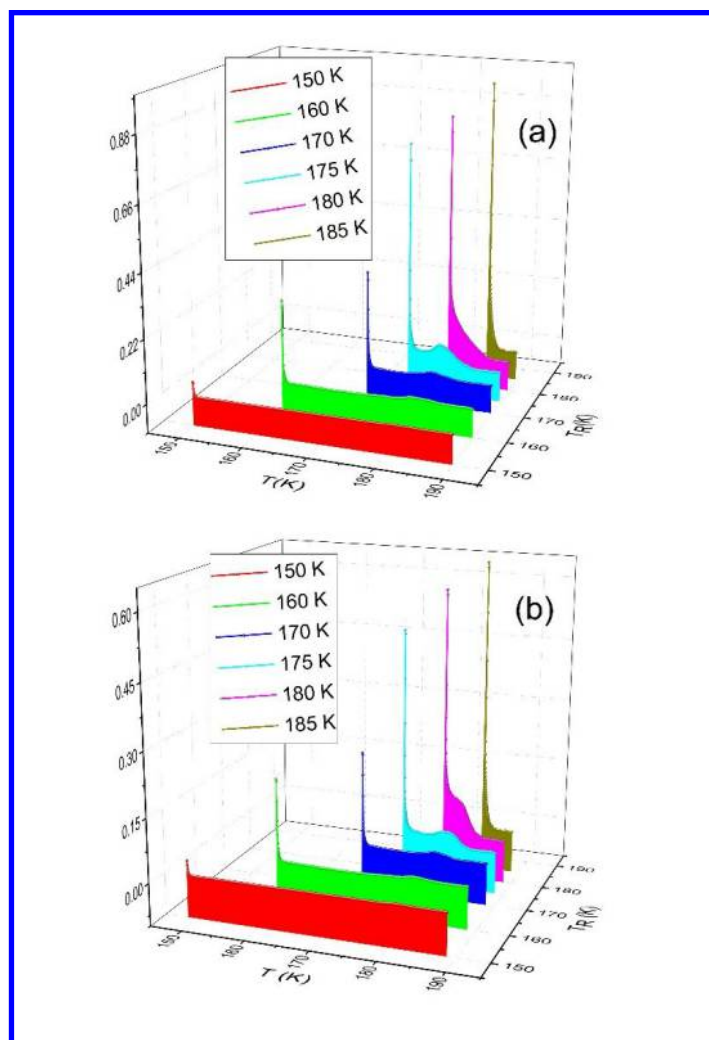


Figure 12 Calorimetric FORC distributions for compound embedded in glassy (a, up) and crystalline matrices (b, down). Note the reversible component (the high peaks) and the irreversible ones.

CONCLUSIONS

1
2
3
4 In this paper, we have analyzed the influence of various glass-forming and semi-
5
6
7 crystalline matrices on the properties of embedded spin-crossover $\text{Fe}(\text{phen})_2(\text{NCS})_2$
8
9
10 microparticles, as reflected in the thermal transition loop based on FORC technique,
11
12
13 applied both to magnetometry and calorimetry experiments. The hypothesis of variable
14
15
16 interactions between spin-crossover particles and matrices has been confirmed by
17
18
19 magnetometric FORCs. The hysteresis shown by spin-crossover microparticles
20
21
22 embedded in matrices is not due to the cooperative elastic interactions between the SC
23
24
25 sites inside the microparticles, but is a result of more or less active interactions with the
26
27
28 matrix depending of its mechanical properties. It is similar with the hysteresis specific to
29
30
31 heterostructures. This work clearly shows that an active matrix could be the path to
32
33
34 follow for a controllable microparticle-switching paradigm. A complementary FORC
35
36
37 method based on calorimetric data, which is essential when the particles actively
38
39
40 interact with the environment, has been proposed, and the results have been
41
42
43 corroborated with magnetometry data. An original treatment of calorimetric FORCs
44
45
46 implying one single derivative has been proposed and should be developed in a future
47
48
49 work.
50
51
52
53
54
55
56
57
58
59
60

1
2
3 Points to be considered should refer to the matrix transformations with respect to the
4
5
6
7 spin crossover and its combination with size reduction and to the investigation of the
8
9
10 effects of light irradiation. The present study can be extended to phase transition in
11
12
13 composite⁵²⁻⁵³ and role of moistening in porous materials like silica or chitosan.⁵⁴⁻⁵⁶
14
15
16
17

18 SUPPORTING INFORMATION

19
20
21

22 TEM image and X-Ray diffractograms of $\text{Fe}(\text{phen})_2(\text{NCS})_2$ in the form of microcrystals.
23
24

25 DSC thermograms of $\text{Fe}(\text{phen})_2(\text{NCS})_2$ microparticles.
26
27
28

29 ACKNOWLEDGMENT

30
31

32 The work was funded by the Romanian Ministry of Research and Innovation within
33
34
35
36 Program 1 - Development of the national RD system, Subprogram 1.22 - Institutional
37
38
39 Performance - RDI excellence funding projects, Contract no.34PFE/19.10.2018 and by
40
41
42 the CNRS, the French Ministry of Research. The collaboration between Romanian and
43
44
45
46 French teams has been supported by PHC Brancusi. DM acknowledges funding from
47
48
49
50 Rennes Metropole and from European FEDER Fund.
51
52
53
54
55
56
57
58
59
60

1
2
3
4 REFERENCES
5
6

- 7 1. Pike, C. R.; Roberts, A. P.; Verosub, K. L., Characterizing Interactions in Fine
8
9
10 Magnetic Particle Systems Using First Order Reversal Curves. *J. Appl. Phys.* **1999**, *85*,
11
12
13
14 6660.
15
16
- 17 2. Stancu, A.; Ricinschi, D.; Mitoseriu, L.; Postolache, P.; Okuyama, M., First-Order
18
19
20 Reversal Curves Diagrams for the Characterization of Ferroelectric Switching. *Appl Phys*
21
22
23
24 *Lett* **2003**, *83*, 3767-3769.
25
26
- 27 3. Pike, C. R.; Roberts, A. P.; Verosub, K. L., First-Order Reversal Curve Diagrams
28
29
30 and Thermal Relaxation Effects in Magnetic Particles. *Geophys. J. Int.* **2001**, *145*, 721.
31
32
33
- 34 4. Enachescu, C.; Tanasa, R.; Stancu, A.; Codjovi, E.; Linares, J.; Varret, F., Forc
35
36
37 Method Applied to the Thermal Hysteresis of Spin Transition Solids: First Approach of
38
39
40
41 Static and Kinetic Properties. *Physica B* **2004**, *343*, 15-19.
42
43
44
- 45 5. Tanasa, R.; Enachescu, C.; Stancu, A.; Linares, J.; Codjovi, E.; Varret, F.;
46
47
48 Haasnoot, J. G., First-Order Reversal Curve Analysis of Spin-Transition Thermal
49
50
51
52 Hysteresis in Terms of Physical-Parameter Distributions and Their Correlations. *Phys.*
53
54
55
56 *Rev. B* **2005**, *71*, 014431.
57
58
59
60

- 1
2
3
4 6. Enachescu, C.; Tanasa, R.; Stancu, A.; Varret, F.; Linares, J.; Codjovi, E., First-
5
6
7 Order Reversal Curves Analysis of Rate-Dependent Hysteresis: The Example of Light-
8
9
10 Induced Thermal Hysteresis in a Spin-Crossover Solid. *Phys. Rev. B* **2005**, *72*, 054413.
11
12
13
14 7. Rotaru, A.; Linares, J.; Varret, F.; Codjovi, E.; Slimani, A.; Tanasa, R.; Enachescu,
15
16
17 C.; Stancu, A.; Haasnoot, J., Pressure Effect Investigated with First-Order Reversal-
18
19
20 Curve Method on the Spin-Transition Compounds $[\text{Fe}_x\text{Zn}_{1-x}(\text{btr})_2(\text{NCS})_2]\text{H}_2\text{O}$ ($x = 0.6, 1$).
21
22
23
24 *Phys. Rev. B* **2011**, *83*, 224107.
25
26
27
28 8. Halcrow, M. A., *Spin-Crossover Materials - Properties and Applications*. John
29
30
31 Wiley & Sons: Chichester, UK, 2013.
32
33
34
35 9. Gütlich, P.; Goodwin, A., *Spin Crossover in Transition Metal Compounds* Springer:
36
37
38 Heidelberg, 2004; Vol. I-III.
39
40
41
42 10. Nicolazzi, W.; Bousseksou, A., Thermodynamical Aspects of the Spin Crossover
43
44
45 Phenomenon. *C. R. Chim.* **2018**, *21*, 1060-1075.
46
47
48
49 11. Boukheddaden, K.; Ritti, M. H.; Bouchez, G.; Sy, M.; Dirtu, M. M.; Parlier, M.;
50
51
52 Linares, J.; Garcia, Y., Quantitative Contact Pressure Sensor Based on Spin Crossover
53
54
55 Mechanism for Civil Security Applications. *J. Phys. Chem. C* **2018**, *122*, 7597-7604.
56
57
58
59
60

- 1
2
3
4 12. Létard, J. F.; Guionneau, P.; Goux-Capes, L., Towards Spin Crossover
5
6
7 Applications. *Top Curr Chem* **2004**, *235*, 221-249.
8
9
- 10 13. Ohkoshi, S.; Imoto, K.; Tsunobuchi, Y.; Takano, S.; Tokoro, H., Light-Induced
11
12 Spin-Crossover Magnet. *Nat. Chem.* **2011**, *3*, 564-569.
13
14
15
16
- 17 14. Enachescu, C.; Machado, H. C.; Menendez, N.; Codjovi, E.; Linares, J.; Varret, F.;
18
19 Stancu, A., Static and Light Induced Hysteresis in Spin-Crossover
20
21 Compounds: Experimental Data and Application of Preisach-Type Models. *Physica B*
22
23
24 **2001**, *306*, 155.
25
26
27
- 28 15. Pillet, S.; Hubsch, J.; Lecomte, C., Single Crystal Diffraction Analysis of the
29
30 Thermal Spin Conversion in [Fe(btr)₂(NCS)₂] (H₂O): Evidence for Spin-Like Domain
31
32 Formation. *Eur. Phys. J. B* **2004**, *38*, 541-552.
33
34
35
36
37
- 38 16. Molnár, G.; Bousseksou, A.; Zwick, A.; McGarvey, J. J., The Spin-Crossover
39
40 Phenomenon in the Solid State: Do Domains Play a Role? A Micro-Raman Study. *Chem*
41
42 . *Phys. Lett.* **2003**, *367*, 593-598.
43
44
45
46
47
48
49
- 50 17. Bonnet, S.; Molnar, G.; Sanchez-Costa, J.; Siegler, A. M.; Spek, A. L.;
51
52 Bousseksou, A.; Fu, W. T.; Gamez, P.; Reedijk, J., Influence of Sample Preparation,
53
54
55
56
57
58
59
60

1
2
3
4 Temperature, Light, and Pressure on the Two-Step Spin Crossover Mononuclear
5
6
7 Compound [Fe(Bapbpy)(NCS)₂]. *Chem. Mater.* **2009**, 1121-1136.
8

9
10 18. Sy, M.; Traiche, R.; Fourati, H.; Singh, Y.; Varret, F.; Boukheddaden, K.,
11
12
13
14 Spatiotemporal Investigations on Light-Driven High-Spin-Low-Spin Interface Dynamics in
15
16
17 the Thermal Hysteresis Region of a Spin-Crossover Single Crystal. *J. Phys. Chem. C*
18
19
20
21 **2018**, *122*, 20952-20962.
22

23
24 19. Tanasa, R.; Enachescu, C.; Stancu, A.; Varret, F.; Linares, J.; Codjovi, E., Study
25
26
27 of Impurities Effect in Spin Crossover Compounds Using First Order Reversal Curves
28
29
30
31 (FORC) Method. *Polyhedron* **2007**, *26*, 1820-1824.
32

33
34
35 20. Stan, R. M.; Gaina, R.; Enachescu, C.; Tanasa, R.; Stancu, A.; Bronisz, R., Kinetic
36
37
38 Effects on Double Hysteresis in Spin Crossover Molecular Magnets Analyzed with First
39
40
41
42 Order Reversal Curve Diagram Technique. *J. Appl. Phys.* **2015**, *117*.
43

44
45 21. Volatron, F.; Catala, L.; Riviere, E.; Gloter, A.; Stephan, O.; Mallah, T., Spin-
46
47
48 Crossover Coordination Nanoparticles. *Inorg. Chem.* **2008**, *47*, 6584.
49

50
51
52 22. Félix, G.; Nicolazzi, W.; Salmon, L.; Molnár, G.; Perrier, M.; Maurin, G.; Larionova,
53
54
55
56 J.; Long, J.; Guari, Y.; Bousseksou, A., Enhanced Cooperative Interactions at the
57
58

1
2
3
4 Nanoscale in Spin-Crossover Materials with a First-Order Phase Transition. *Phys. Rev.*
5
6
7 *Lett.* **2013**, *110*, 235701.

8
9
10 23. Raza, Y., et al., Matrix-Dependent Cooperativity in Spin Crossover
11
12
13 Fe(Pyrazine)Pt(Cn)₄ Nanoparticles *Chem. Commun.* **2011**, *47*, 11501-11503.

14
15
16
17 24. Rotaru, A.; Varret, F.; Gindulescu, A.; Linares, J.; Stancu, A.; Létard, J. F.;
18
19
20 Forestier, T.; Etrillard, C., Size Effect in Spin-Crossover Systems Investigated by Forc
21
22
23 Measurements, for Surfacted [Fe(NH₂-Trz)₃](Br)₂·3H₂O Nanoparticles: Reversible
24
25
26
27 Contributions and Critical Size. *Eur. Phys. J. B* **2011**, *84*, 439-449.

28
29
30
31 25. Stoleriu, L.; Chakraborty, P.; Hauser, A.; Stancu, A.; Enachescu, C., Thermal
32
33
34 Hysteresis in Spin-Crossover Compounds Studied within the Mechanoelastic Model and
35
36
37 Its Potential Application to Nanoparticles. *Phys. Rev. B* **2011**, *84*, 134102.

38
39
40
41 26. Mikolasek, M.; Felix, G.; Peng, H.; Rat, S.; Terki, F.; Chumakov, A. I.; Salmon, L.;
42
43
44 Molnár, G.; Nicolazzi, W.; Bousseksou, A., Finite-Size Effects on the Lattice Dynamics in
45
46
47 Spin Crossover Nanomaterials. I. Nuclear Inelastic Scattering Investigation. *Phys Rev B*
48
49
50
51 **2017**, *96*, 035426.

- 1
2
3
4 27. Felix, G.; Mikolasek, M.; Molnar, G.; Nicolazzi, W.; Bousseksou, A., Tuning the
5
6
7 Spin Crossover in Nano-Objects: From Hollow to Core-Shell Particles. *Chemi. Phys. Lett.*
8
9
10 **2014**, *607*, 10-14.
11
12
13
14 28. Oubouchou, H.; Singh, Y.; Boukheddaden, K., Magnetoelastic Modeling of Core-
15
16
17 Shell Spin-Crossover Nanocomposites. *Phys. Rev. B* **2018**, *98*.
18
19
20
21 29. Atitoaie, A.; Tanasa, R.; Stancu, A.; Enachescu, C., Study of Spin Crossover
22
23
24 Nanoparticles Thermal Hysteresis Using FORC Diagrams on an Ising-Like Model. *J.*
25
26
27 *Magn. Magn. Mater.* **2014**, *368*, 12-18.
28
29
30
31 30. Tissot, A.; Enachescu, C.; Boillot, M. L., Control of the Thermal Hysteresis of the
32
33
34 Prototypal Spin-Transition $\text{Fe}_{ii}(\text{Phen})_2(\text{Ncs})_2$ Compound Via the Microcrystallites
35
36
37 Environment: Experiments and Mechanoelastic Model *J. Mater. Chem.* **2012**, *22*, 20451-
38
39
40
41 20457.
42
43
44
45 31. Tanasa, R.; Laisney, J.; Stancu, A.; Boillot, M. L.; Enachescu, C., Hysteretic
46
47
48 Behavior of $\text{Fe}(\text{Phen})_2(\text{Ncs})_2$ Spin-Transition Microparticles Vs. The Environment: A
49
50
51 Huge Reversible Component Resolved by First Order Reversal Curves. *Appl. Phys. Lett.*
52
53
54
55 **2014**, *104*, 031909.
56
57
58
59
60

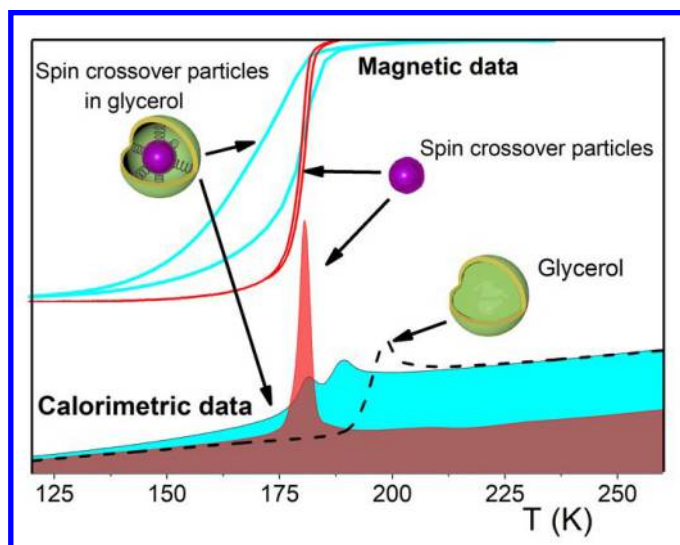
- 1
2
3
4 32. Enachescu, C.; Tanasa, R.; Stancu, A.; Tissot, A.; Laisney, J.; Boillot, M. L., Matrix-
5
6
7 Assisted Relaxation in Fe(Phen)₂(NCS)₂ Spin-Crossover Microparticles, Experimental
8
9
10 and Theoretical Investigations. *Appl Phys Lett* **2016**, *109*.
- 11
12
13
14 33. Laisney, J.; Tissot, A.; Molnar, G.; Rechinat, L.; Rivière, E.; Brisset, F.;
15
16
17 Bousseksou, A.; Boillot, M. L., Nanocrystals of Fe(Phen)₂(NCS)₂ and the Size-
18
19
20 Dependent Spin-Crossover Characteristics. *Dalton Trans.* **2015**, *44*, 17302-17311
- 21
22
23
24 34. Fishman, A. I.; Noskov, A. I.; Stolov, A. A., Conformational Mobility of Small
25
26
27 Molecules in Glass-Forming Solutions Studied by Ftir Spectroscopy. *Spectrochim. Acta*
28
29
30
31 *A* **2012**, *91*, 184.
- 32
33
34
35 35. Chelli, R.; Procacci, P.; Cardini, G.; Della Valle, R. G.; Califano, S., Glycerol
36
37
38 Condensed Phases Part I. A Molecular Dynamics Study *Phys. Chem. Chem. Phys.* **1999**,
39
40
41
42 *1*, 871.
- 43
44
45 36. Martin, J. P.; Zarembowitch, J.; Bousseksou, A.; Dworkin, A.; Haasnoot, J.; Varret,
46
47
48 F., Solid State Effects on Spin Transitions: Magnetic, Calorimetric, and Moessbauer-
49
50
51 Effect Properties of [Fe_xCo_{1-x}(4,4'-bis-1,2,4-Triazole)₂(NCS)₂].H₂O Mixed-Crystal
52
53
54
55 Compounds. *Inorg. Chem.* **1994**, *33*, 6325-6333.
- 56
57
58
59
60

- 1
2
3
4 37. Rotaru, A.; Dirtu, M. M.; Enachescu, C.; Tanasa, R.; Linares, J.; Stancu, A.; Garcia,
5
6
7 Y., Calorimetric Measurements of Diluted Spin Crossover Complexes [FexM_{1-x}(btr)₂(NCS)₂]H₂O with M_{ii} = Zn and Ni. *Polyhedron* **2009**, *28*, 2351-2356.
8
9
10
11
12
13
14 38. Sorai, M.; Nakano, M.; Miyazaki, Y., Calorimetric Investigation of Phase
15
16
17 Transitions Occurring in Molecule-Based Magnets. *Chem. Rev.* **2006**, *106*, 976-1031.
18
19
20
21 39. Castro, M.; Roubreau, O.; Pineiro-Lopez, L.; Real, J. A.; Rodriguez-Velamazán, J.
22
23
24 A., Pulsed-Laser Switching in the Bistability Domain of a Cooperative Spin Crossover
25
26
27 Compound: A Critical Study through Calorimetry. *J. Phys. Chem. C* **2015**, *119*, 17334-
28
29
30
31 17343.
32
33
34
35 40. Sorai, M.; Seki, S., Phonon Coupled Cooperative Low-Spin 1a1high-Spin 5t2
36
37
38 Transition in [Fe(phen)₂(NCS)₂] and [Fe(phen)₂(NCSe)₂] Crystals. *J. Phys. Chem. Solids*
39
40
41 **1974**, *35*, 555.
42
43
44
45 41. Zheng, W.; Simon, S. L., Confinement Effects on the Glass Transition of Hydrogen
46
47
48 Bonded Liquids. *J. Chem. Phys.* **2007**, *127*.
49
50
51
52
53
54
55
56
57
58
59
60

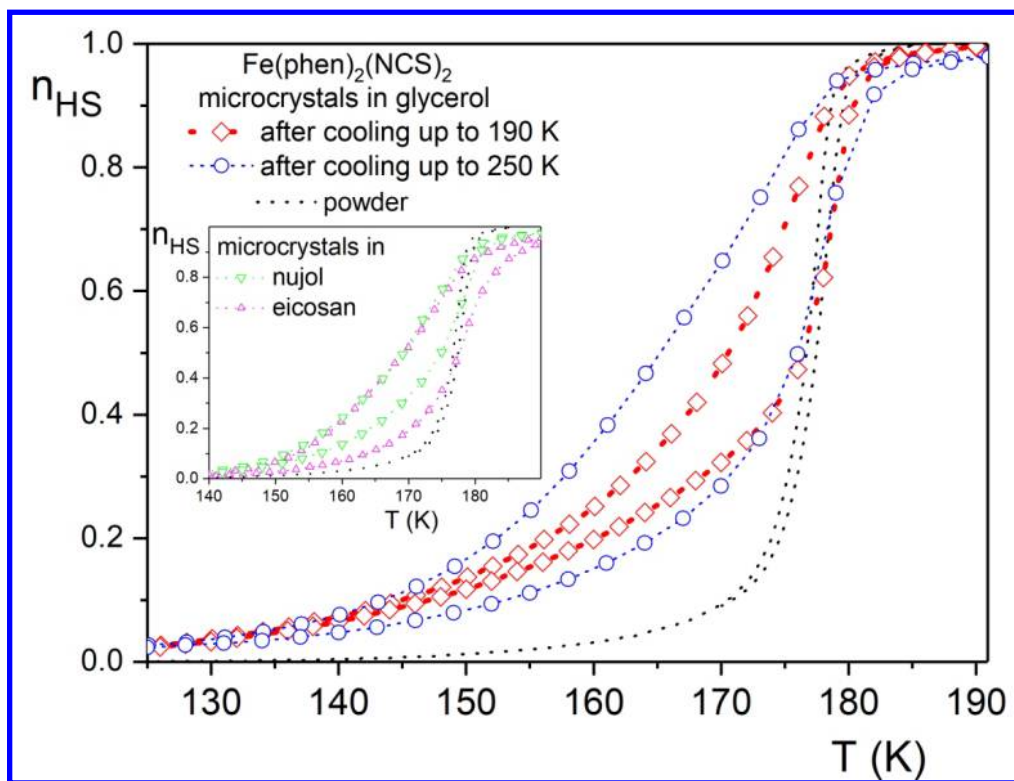
- 1
2
3
4 42. Roux, C.; Zarembowitch, J.; Itie, J. P.; Polian, A.; Verdaguer, M., Pressure-Induced
5
6
7 Spin-State Crossovers in Six-Coordinate Fe(II)L(N)L'(M)(NCS)₂ Complexes with L=L'
8
9
10 and L Not Equal L': A XANES Investigation. *Inorg Chem* **1996**, *35*, 574-580.
11
12
13
14 43. Riggleman, R. A.; de Pablo, J. J., Antiplasticization and Local Elastic Constants in
15
16
17 Trehalose and Glycerol Mixtures. *Journal of Chemical Physics* **2008**, *128*, 224504.
18
19
20
21 44. Ediger, M. D.; Angell, C. A.; Nagel, S. R., Supercooled Liquids and Glasses. *J.*
22
23
24 *Phys. Chem.* **1996**, *100*, 13200-13212.
25
26
27
28 45. Willart, J. F.; Dudognon, E.; Mahieu, A.; Eddleston, M.; Jones, W.; Descamps, M.,
29
30
31 The Role of Cracks in the Crystal Nucleation Process of Amorphous Griseofulvin. *Eur.*
32
33
34 *Phys. J.-Special Topics* **2017**, *226*, 837-847.
35
36
37
38 46. Mayergoyz, D., *Mathematical Models of Hysteresis*; Springer, New York, 1991.
39
40
41
42 47. Stancu, A.; Pike, C. R.; Stoleriu, L.; Postolache, P.; Cimpoesu, D., Micromagnetic
43
44
45 and Preisach Analysis of the First Order Reversal Curves (FORC) Diagram. *J. Appl. Phys.*
46
47
48 **2003**, *93*, 6620-6622.
49
50
51
52
53
54
55
56
57
58
59
60

- 1
2
3
4 48. Nguyen, L. L.; Guillot, R.; Laisney, J.; Rechinat, L.; Bedoui, S.; Molnar, G.;
5
6
7 Rivière, E.; Boillot, M. L., Fe(Me₂-bpy)₂(NCSe)₂ Spin-Crossover Micro- and Nanoparticles
8
9
10 Showing Spin-State Switching above 250 K *New. J. Chem.* **2015**, *39*, 1603-1610.
11
12
13
14 49. Stoleriu, L.; Enachescu, C., Elastic Model for Spin Crossover Nanoparticles in
15
16
17 Matrices *Proc. Ro. Acad. Series A* **2019**, *20*, 59-66.
18
19
20
21 50. Yokogawa, K.; Murata, K.; Yoshino, H.; Aoyama, S., Solidification of High-
22
23
24 Pressure Medium Daphne 7373. *Jpn J. Appl. Phys.* **2007**, *46*, 3636-3639.
25
26
27
28 51. Abou Hamad, I.; Robb, D. T.; Rikvold, P. A., New Cyclic Voltammetry Method for
29
30
31 Examining Phase Transitions: Simulated Results. *Journal of Electroanalytical Chemistry*
32
33
34 **2007**, *607*, 61-68.
35
36
37
38 52. Chen, M. Y.; Chen, X. R.; Ning, W. H.; Ren, X. M., A Facile Route for Preparation
39
40
41 of Monodisperse Nanoparticles of One-Dimensional Fe(II)-4-Amino-1,2,4-Triazole
42
43
44 Coordination Polymers with Hysteretic Spin-Crossover near Room Temperature. *RSC*
45
46
47 *Advances* **2014**, *4*, 39126-39131.
48
49
50
51
52
53
54
55
56
57
58
59
60

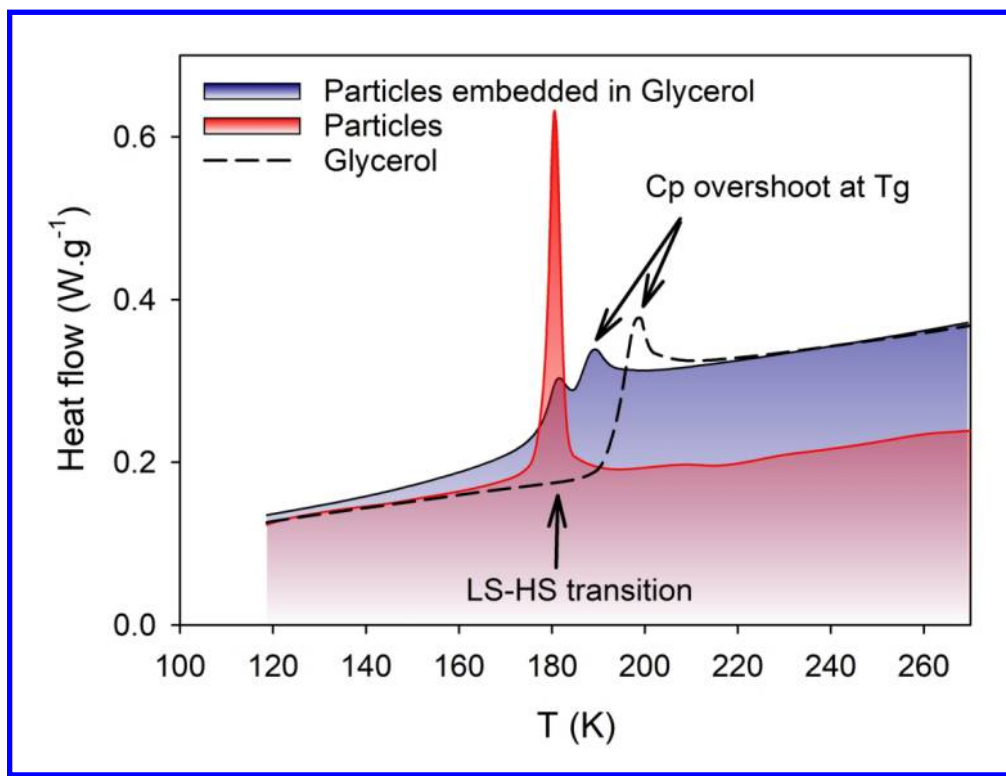
- 1
2
3
4 53. Bartual-Murgui, C.; Natividad, E.; Roubeau, O., Critical Assessment of the Nature
5
6
7 and Properties of Fe(II) Triazole-Based Spin-Crossover Nanoparticles. *J. Mater. Chem.*
8
9
10 *C* **2015**, *3*, 7916-7924.
11
12
13
14 54. Voisin, H.; Aimé, C.; Vallée, A.; Bleuzen, A.; Schmutz, M.; Mosser, G.; Corradin,
15
16
17 T.; Roux, C., Preserving the Spin Transition Properties of Iron-Triazole Coordination
18
19
20 Polymers within Silica-Based Nanocomposites. *J. Mater. Chem. C* **2017**, *5*, 11542-11550.
21
22
23
24 55. Durand, P., et al., Room Temperature Bistability with Wide Thermal Hysteresis in
25
26
27 a Spin Crossover Silica Nanocomposite. *J. Mater. Chem. C* **2013**, *1*, 1933-1942.
28
29
30
31 56. Herrera, J. M., et al., Studies on Bifunctional Fe(II)-Triazole Spin Crossover
32
33
34 Nanoparticles: Time-Dependent Luminescence, Surface Grafting and the Effect of a
35
36
37 Silica Shell and Hydrostatic Pressure on the Magnetic Properties. *J. Mater. Chem. C*
38
39
40
41 **2015**, *3*, 7819-7829.
42
43
44
45
46
47
48
49
50
51
52
53
54
55
56
57
58
59
60



TOC graphic

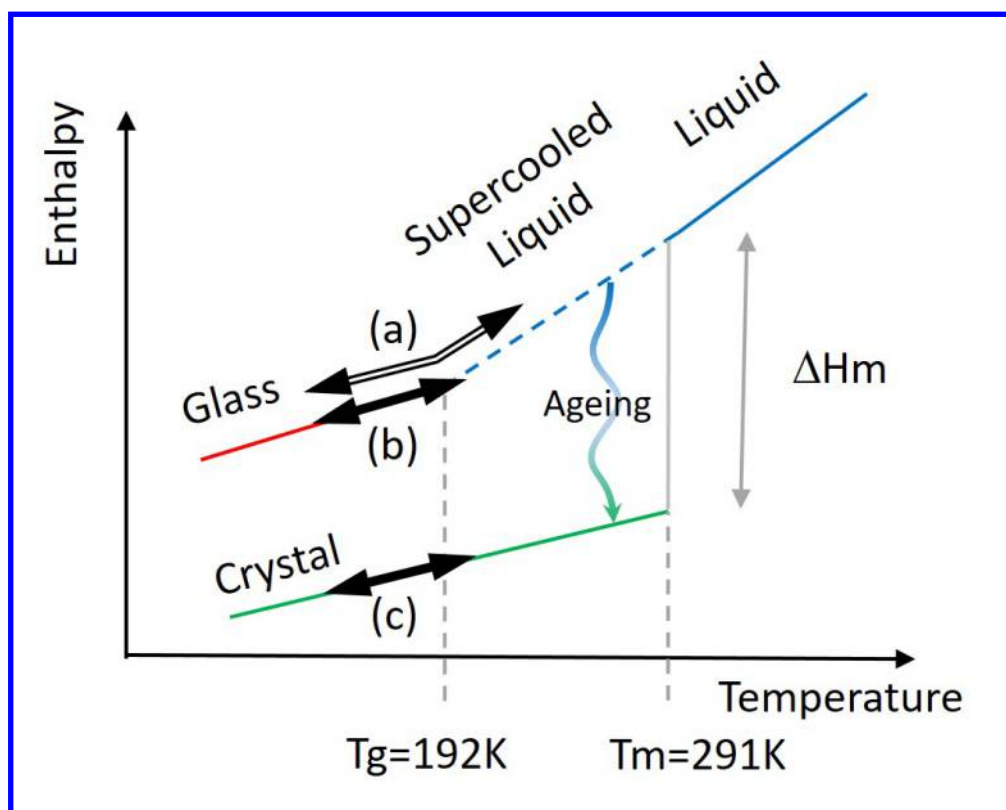


Major hysteresis loop (MHL) for $Fe(phen)_2(NCS)_2$ as polycrystalline powder (dotted line) and as dispersions of crystalline microparticles in glycerol after a first cooling down and heating up to 190 or 250 K (main figure) and as dispersions of crystalline microparticles in nujol and eicosan after a first cooling down and heating up to 190K (inset).

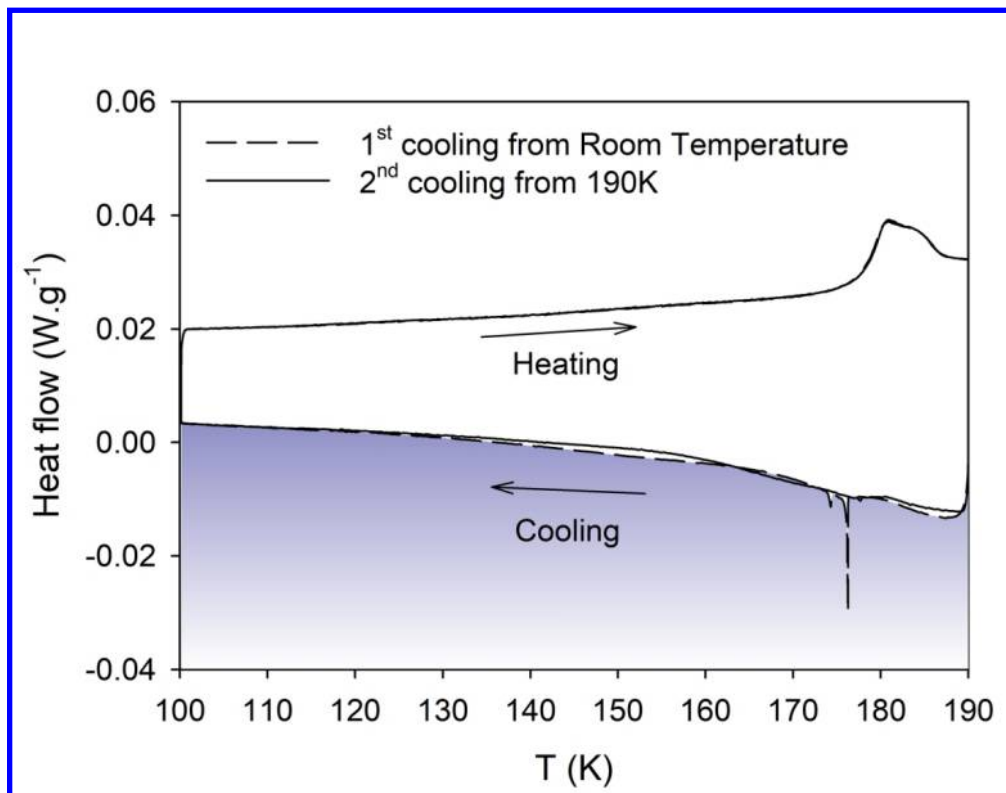


DSC thermograms recorded on heating after a first cooling down from 273 to 110 K, with a temperature scanning rate of 10 K·min⁻¹ for pure glycerol (dashed line), free Fe(phen)₂(NCS)₂ microparticles (blue shaded) and Fe(phen)₂(NCS)₂ microparticles embedded in glycerol (red line).

157x119mm (300 x 300 DPI)



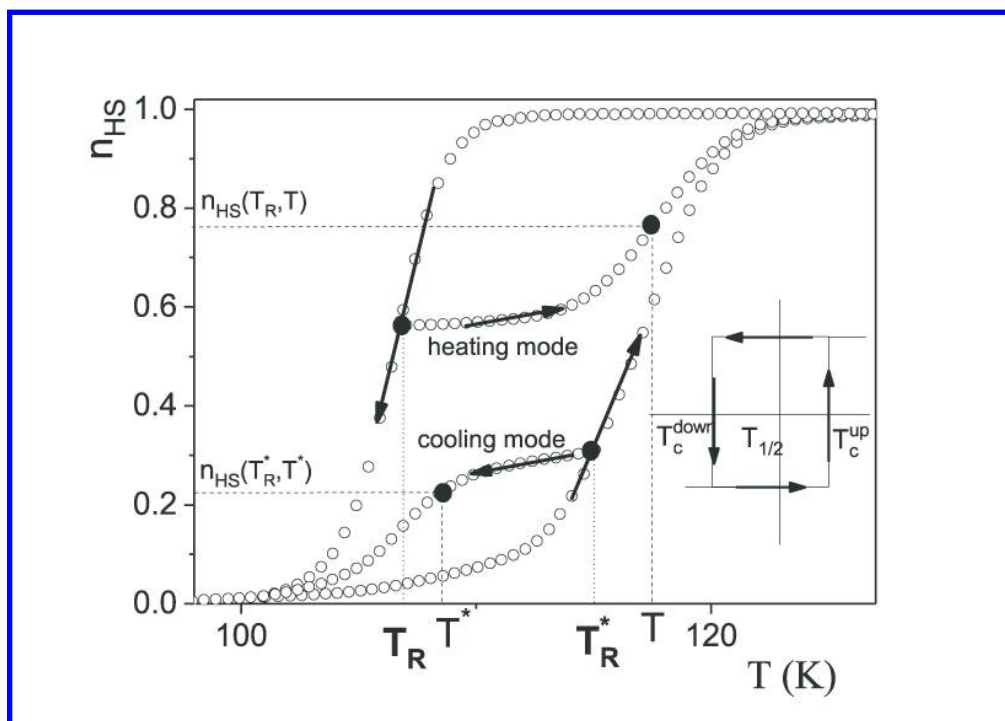
Schematic representation of glycerol stable and metastable phases. The thermal treatments are shown by arrows: (a) cycling in the glassy and liquid phases in the range 100-250 K, (b) cycling in glassy phase 100-190 K, and (c) cycling in the crystal 100-190 K



31
32
33
34
35
36
37
38
39
40
41
42
43
44
45
46
47
48
49
50
51
52
53
54
55
56
57
58
59
60

DSC thermograms of $\text{Fe}(\text{phen})_2(\text{NCS})_2$ microparticles embedded in glycerol recorded with a temperature scanning rate of $0.5 \text{ K}\cdot\text{min}^{-1}$ and with different cycling conditions. The two lower curves correspond to the cooling branches: a first cooldown after having heated the system above 250 K (dashed line) and a subsequent cooldown after heating up to 190 K (solid line). The two upper curves correspond to the heating branches (superimposed solid lines).

158x123mm (300 x 300 DPI)



Examples of FORCs in warming and cooling modes; inset: typical hysteron for cooperative interactions

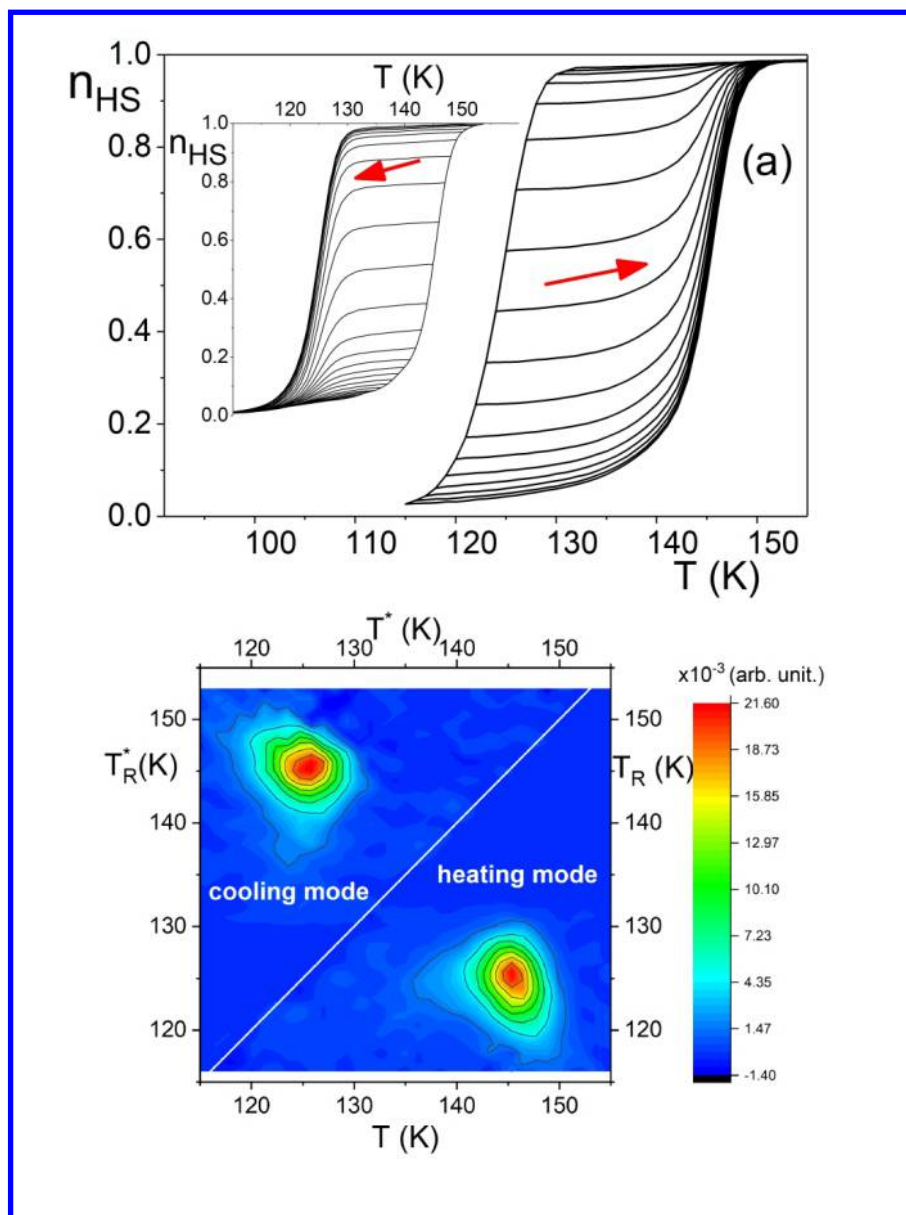
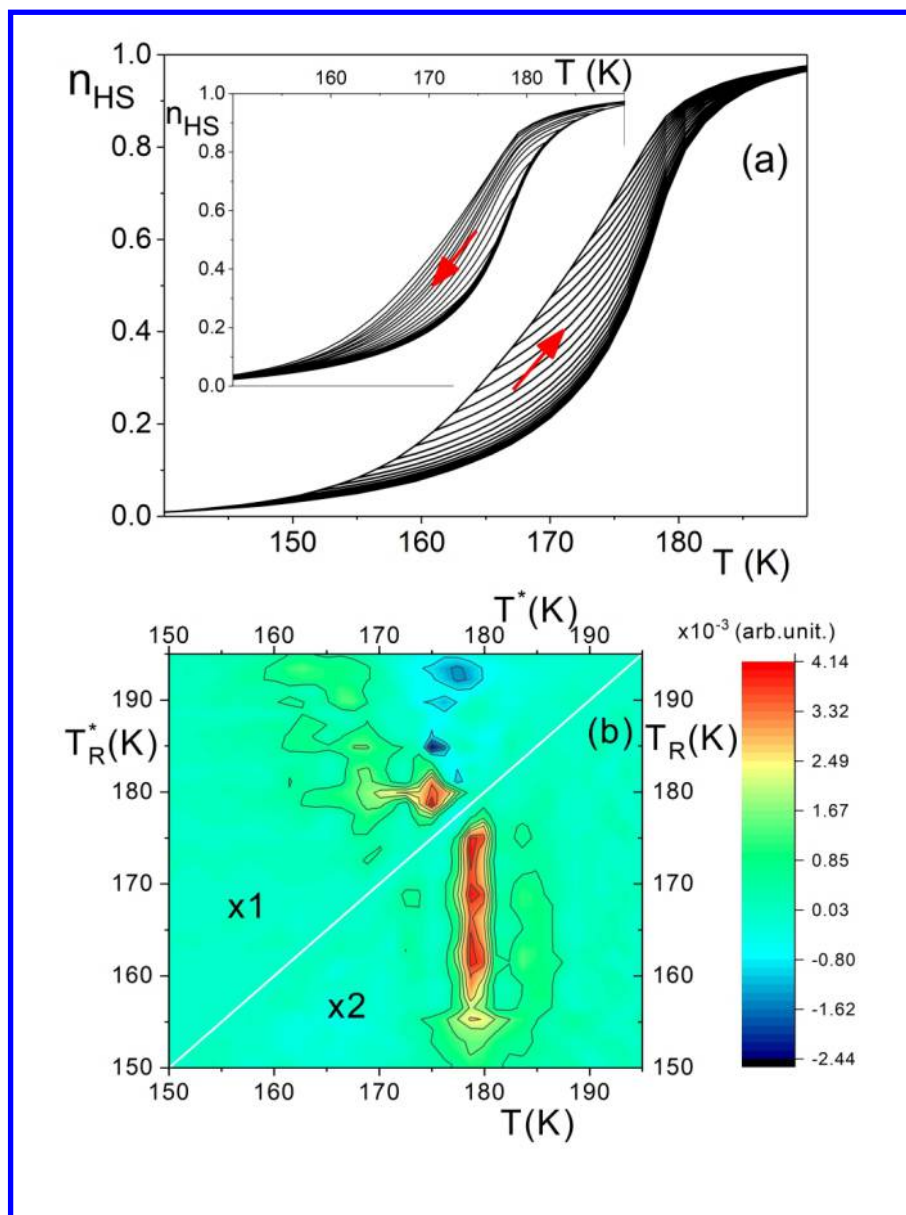
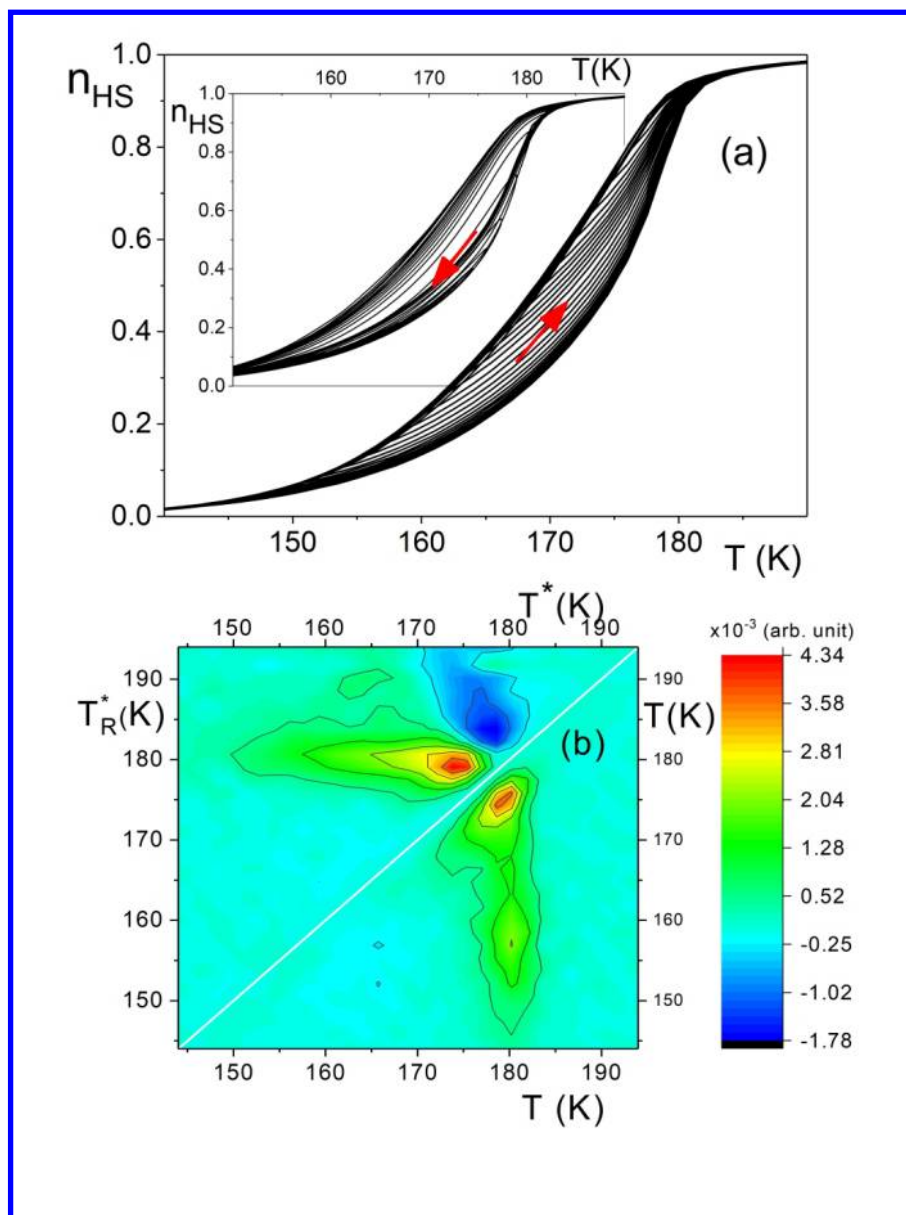


Figure 6 Typical FORCs in the case of powder spin-crossover compound $[\text{Fe}(\text{btr})_2(\text{NCS})_2] \cdot \text{H}_2\text{O}$ 5 (a) Main figure: heating mode, inset: cooling mode. (b) FORC distributions for heating (lower side) and cooling modes (upper side).

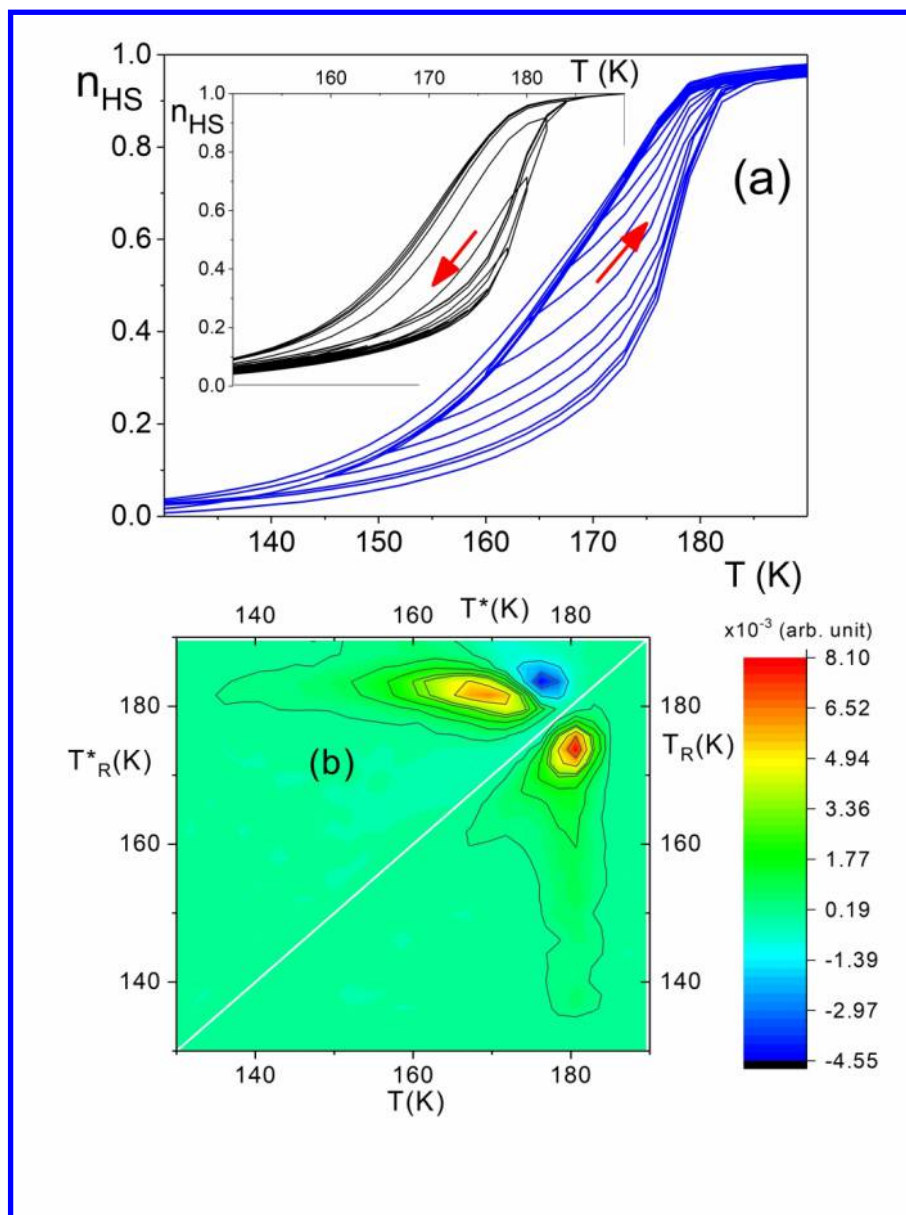
359x480mm (300 x 300 DPI)



FORCs for Fe(phen)₂(NCS)₂ microparticles embedded in eicosan. (a) Main figure: heating mode (T_{up} = 190 K), inset: cooling mode, T_{down} = 140 K). (b) FORC distributions for heating (lower side, multiplied by 2) and cooling modes (upper side).



FORCs for Fe(phen)₂(NCS)₂ microparticles embedded in nujol. (a) Main figure: heating mode (T_{up}=190 K), inset: cooling mode (T_{down} = 140 K). (b) FORC distributions for heating (lower side) and cooling modes (upper side).



(a) FORCs for $\text{Fe}(\text{phen})_2(\text{NCS})_2$ microparticles embedded in glycerol for warming mode when cycling up to 250 K, (main figure) and cooling modes (inset) (b) Corresponding FORC distributions. The temperature scan rate was $0.3 \text{ K}\cdot\text{min}^{-1}$.

359x480mm (300 x 300 DPI)

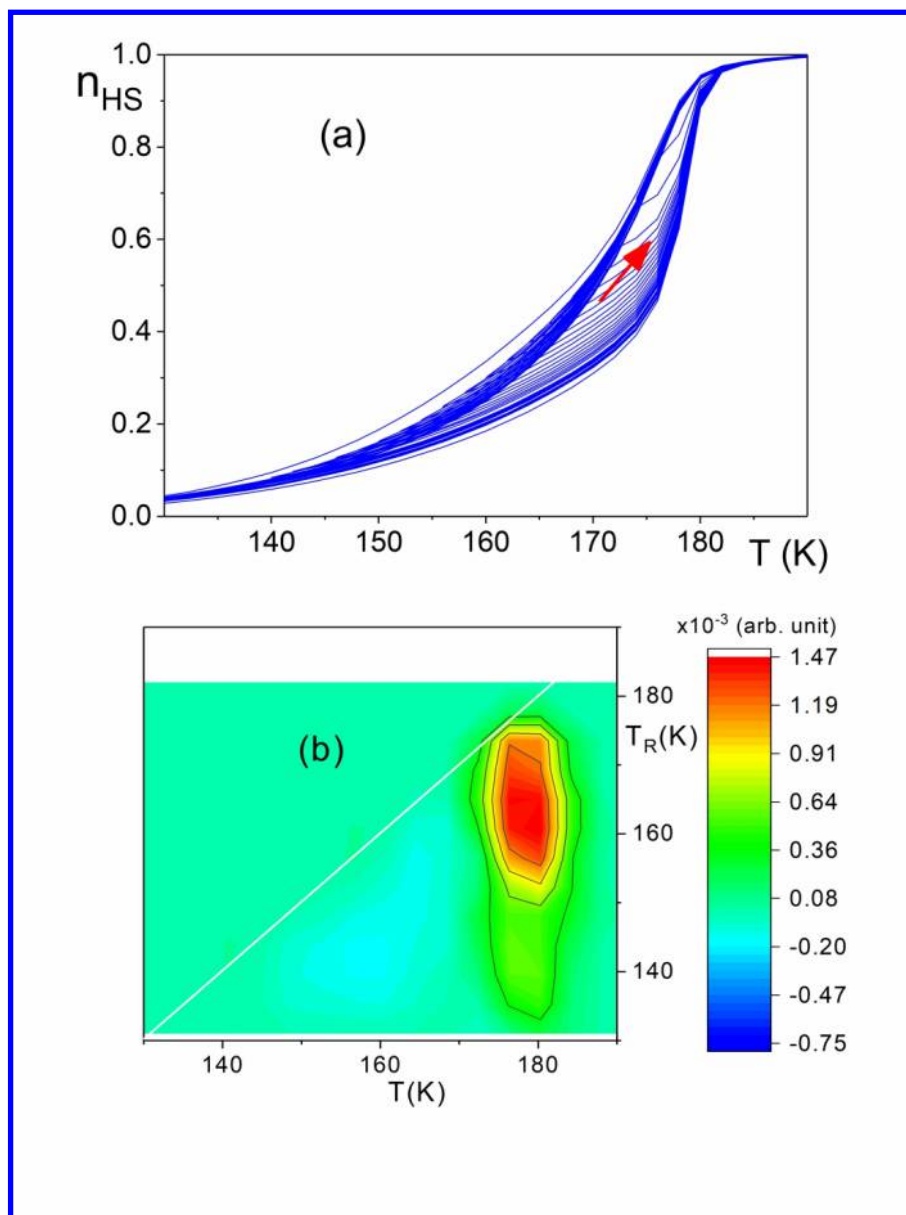
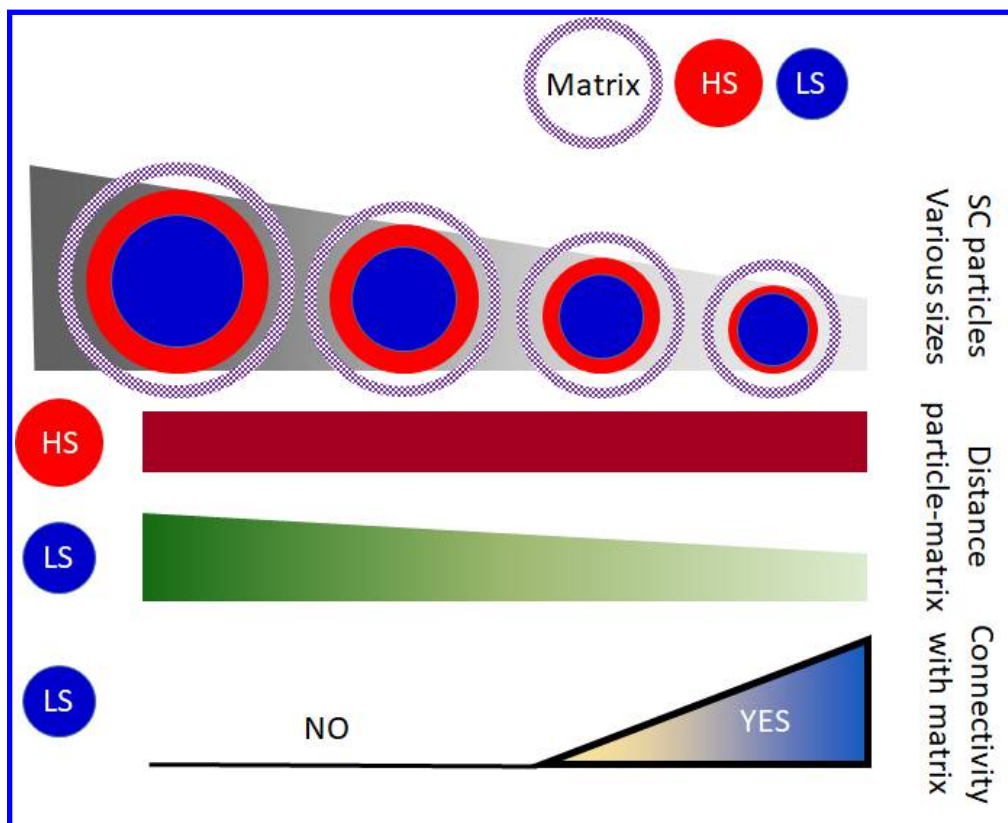


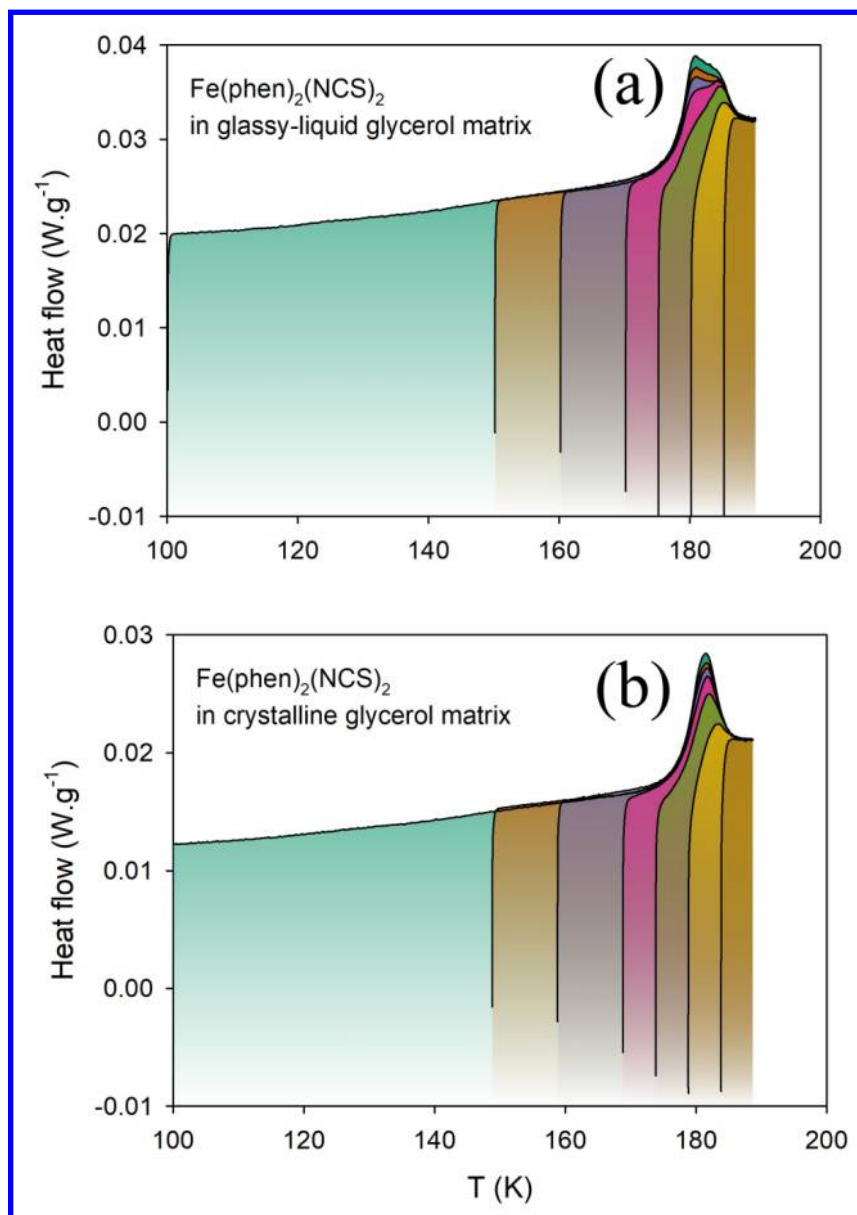
Figure 10 (a) FORCs for Fe(phen)₂(NCS)₂ microparticles embedded in glycerol for warming mode when cycling up to 190 K (main figure) (b) Corresponding FORC distributions. The temperature scan rate was 0.3 K·min⁻¹.

359x480mm (300 x 300 DPI)

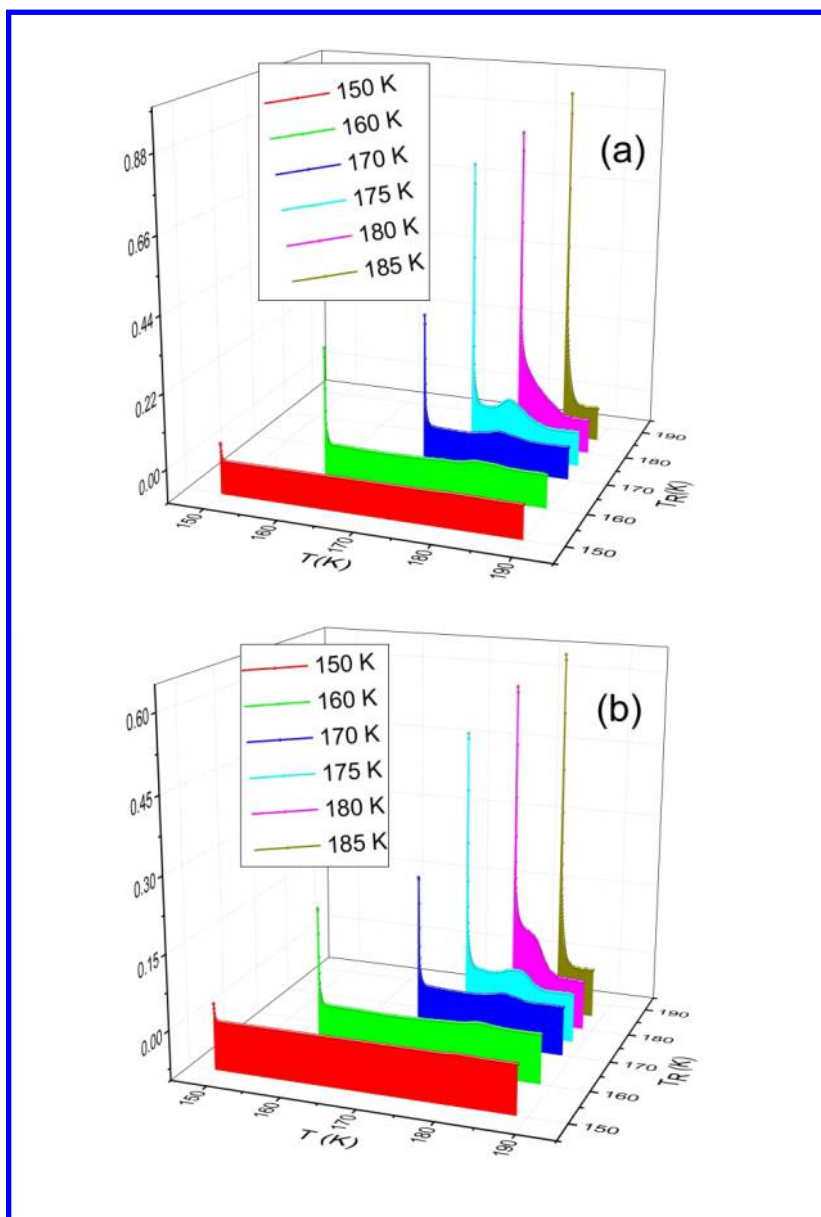


Schematic representation of particle-matrix interactions during HS-LS transition

243x196mm (72 x 72 DPI)



First Order Reversal Curves DSC thermograms in the heating mode for composites of Fe(phen)₂(NCS)₂ microparticles embedded in glassy (a) and crystalline (b) glycerol.



Calorimetric FORC distributions for compound embedded in glassy (a, up) and crystalline matrices (b, down). Note the reversible component (the high peaks) and the irreversible ones.